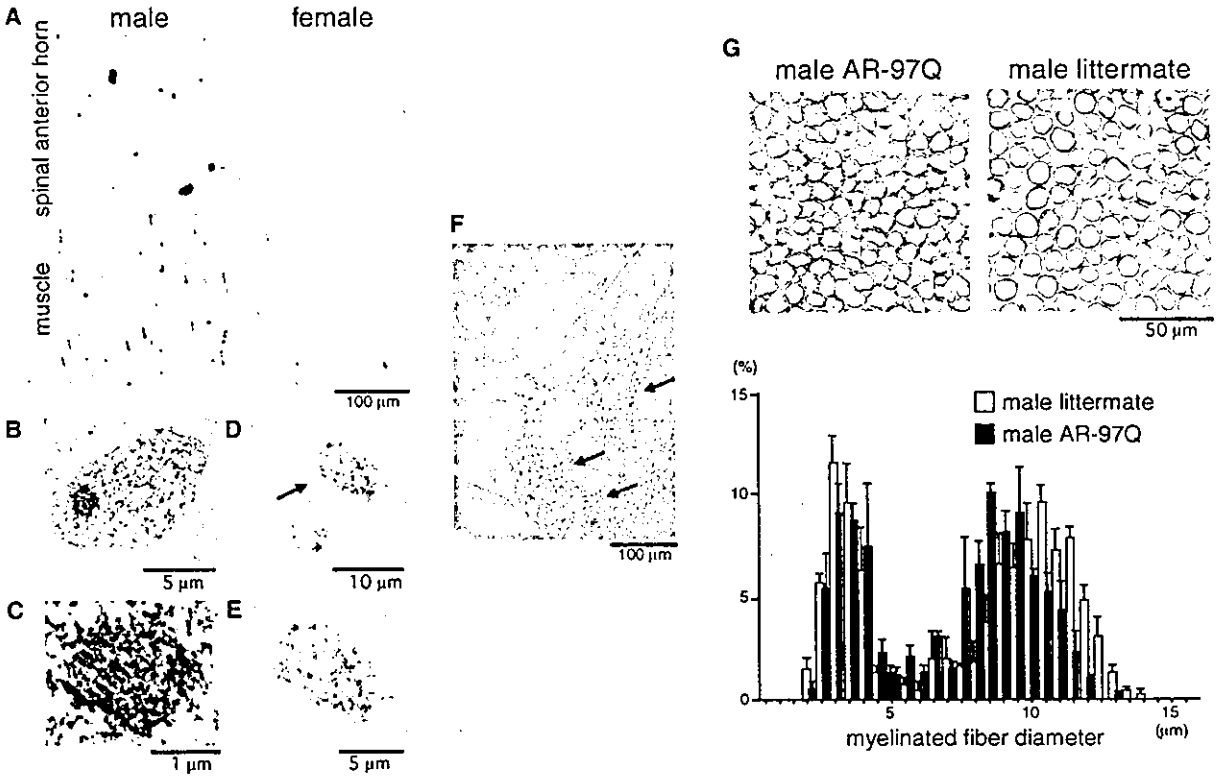

Figure 2. Pathologic Findings of AR-97Q Mice

(A) Immunohistochemical study of the spinal anterior horn and muscle of the male and female AR-97Q mice stained with a monoclonal antibody (1C2) against abnormally expanded polyglutamine (#7–8, 14-week-old). (B–E) Electron microscopic immunohistochemistry for 1C2 of an anterior horn cell (#4–6, 24-week-old). Dense granular aggregate of 1C2-immunoreactive material was recognized in the motor neuron nucleus which showed a nuclear inclusion in light micrograph (B, low magnification and C, high magnification). Another motor neuron (D, arrow), which demonstrated diffuse nuclear staining in light micrograph, showed microaggregates in high magnification (E). (F) HE staining of the muscle in the male AR-97Q mouse revealed obvious grouped atrophy and small angulated fibers (arrow) (#7–8, 14-week-old). (G) Toluidine blue staining and the histogram of myelinated fiber diameter of the L5 ventral root of male AR-97Q mice and their normal littermates. Large myelinated fibers in the ventral root showed axonal atrophy in the male AR-97Q mice (■, n = 3) compared with normal littermates (□, n = 3) (#7–8, 13-week-old).

male AR-97Q mice showed significantly more diffuse nuclear staining and NIs than females in agreement with the symptomatic and Western blot profile differences with gender (Table 2, Figure 2A). Electron microscopic immunohistochemistry for 1C2 demonstrated granular aggregates corresponding to NIs and fine microaggregates corresponding to diffuse nuclear staining in the neuronal tissues (Figures 2B–2E).

Muscle histology revealed significant grouped atrophy and small angulated fibers in the male AR-97Q mice as well as mild myopathic change such as increased variability in muscle fiber size (Figure 2F). Although the number of spinal motor neurons tended to be reduced in AR-97Q mice, the difference was not significant; 452 ± 10/10 sections in L5 segment of AR-97Q mice and 543 ± 28/10 sections in their littermates ($p = 0.10$). Nevertheless, the cross-sectional area of the individual spinal motor neurons significantly decreased in the male AR-97Q mice: 130.6 ± 4.0 μm^2 in L5 of male AR-97Q and 195.6 ± 12.1 μm^2 in their male littermates ($p = 0.006$). In addition, the diameter of large myelinated fibers (≥6.0 μm) was significantly diminished in the male AR-97Q mice (Figure 2G); the diameter of large fibers of the L5 ventral root was 8.49 ± 0.27 μm in male AR-97Q and 10.29 ± 1.08 μm in their male littermates ($p = 0.05$), whereas that of small fibers (<6.0 μm) was 3.11 ± 0.23 μm in male AR-97Q and 2.86 ± 0.11 μm in their male littermates ($p = 0.16$). Female AR-97Q mice showed no neuropathic changes. Neuronal cell population in the cerebrum, cerebellum, and dorsal root ganglia was fairly well preserved despite the abundant diffuse nuclear staining and NIs (data not shown).

Castration Prevents Phenotypic Expression in Male AR-97Q Mice

Castrated male AR-97Q mice showed marked improvement of symptoms, pathologic findings, and nuclear localization of the mutant AR compared with the sham-operated male AR-97Q mice. These castrated male AR-97Q mice weighed the same as their castrated male littermates, whereas the sham-operated male AR-97Q mice showed progressive emaciation (Figure 3A). Motor impairment assessed by rotarod and cage activity was significantly less or virtually absent in the castrated male AR-97Q mice as compared with the sham-operated male AR-97Q mice (Figures 3B and 3C). The castrated male AR-97Q mice showed motor impairment similar to that of the female AR-97Q mice. The life span was also

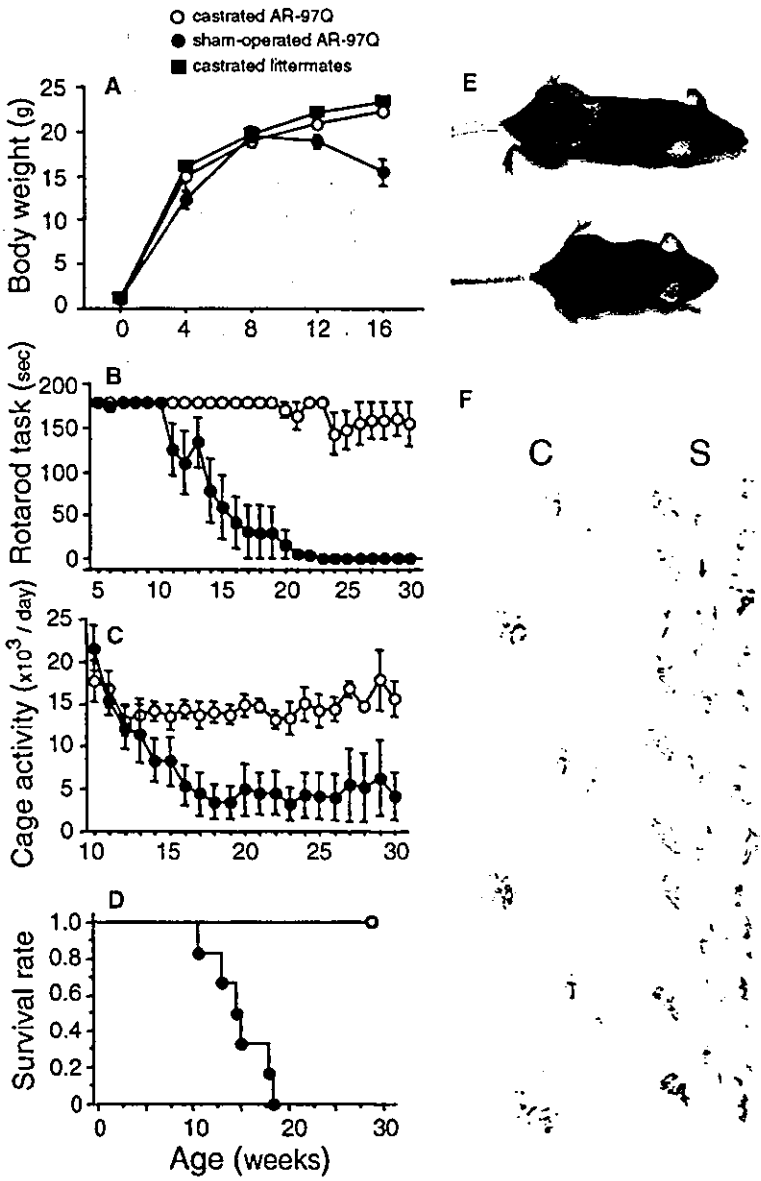

Figure 3. Effects of Castration on the Symptomatic Phenotypes of Male AR-97Q Mice

(A–D) Body weight (A, #7–8), rotarod task (B, #7–8), cage activity (C, #7–8), and survival rate (D, #2–6) of the castrated (○, n = 6) and sham-operated (●, n = 6) male AR-97Q mice. All parameters are significantly different between the sham-operated male AR-97Q mice and the castrated male AR-97Q mice or castrated male littermates (■, n = 2) ($p = 0.0001$, $p < 0.0001$, $p = 0.006$, and $p = 0.0006$, respectively). (E) The castrated AR-97Q mouse (top) shows no muscular atrophy, which is striking in the sham-operated male AR-97Q mouse (bottom) (#2–6, 12-week-old). (F) Footprints of 12-week-old castrated (C) and sham-operated (S) male AR-97Q mice (#2–6). Front paws are in red, and hind paws in blue paint.

significantly prolonged in the castrated male AR-97Q mice (Figure 3D). The castrated AR-97Q mice showed amelioration of muscle atrophy and body size reduction (Figure 3E). In a footprint analysis, the sham-operated male AR-97Q mice exhibited motor weakness with dragging of their hindlegs, which improved in the castrated male AR-97Q mice (Figure 3F). In the Western blot analysis using N-20, the mutant AR appearing within the stacking gel was markedly diminished in the castrated male AR-97Q mice compared with the sham-operated male AR-97Q mice (Figure 4A). The mutant AR in the nuclear fraction also significantly decreased in the castrated male AR-97Q mice (Figure 4B). The castrated male AR-97Q mice showed markedly diminished diffuse nuclear staining and NIs (Figure 4C). These observations suggested that castration markedly prevented nuclear localization of the mutant AR protein. The serum testosterone in the castrated male AR-97Q mice dramatically decreased to an undetectable low level, whereas that in sham-operated male AR-97Q mice was 27.7 ± 1.2 ng/dl (#7–8, n = 4).

Testosterone Administration Deteriorates Phenotypic Expression in Female Tg Mice

By contrast, testosterone administration markedly exacerbated symptoms, pathologic features, and nuclear localization of the mutant AR in the female AR-97Q mice. The testosterone-administered female AR-97Q mice showed progressive emaciation (Figure 5A). The motor impairment assessed by rotarod and cage activity was significantly worsened in the female AR-97Q mice administered testosterone, being similar to those of the untreated male AR-97Q mice (Figures 5B and 5C). The life span of the female AR-97Q mice was also affected by testosterone administration (Figure 5D). The testosterone-administered AR-97Q mice showed marked muscle atrophy and body size reduction (Figure 5E). In a footprint analysis, the testosterone-administered

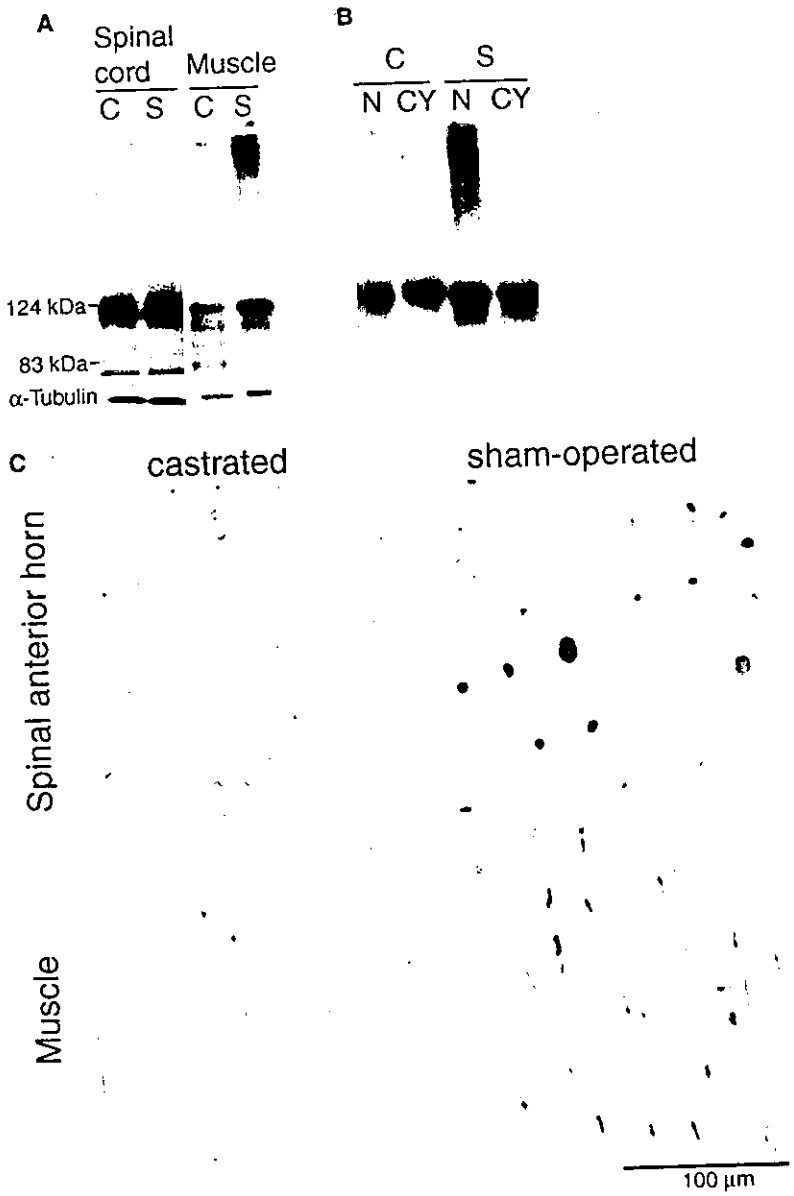

Figure 4. Effects of Castration on Transgene Expression and Neuropathology of Male AR-97Q Mice

(A) Western blot analysis of total homogenates from the spinal cord and muscle of the castrated (C) and sham-operated (S) male AR-97Q mice, which were immunolabeled by N-20 (#7–8, 13-week-old). (B) Western blot analysis of nuclear (N) and cytoplasmic (CY) fraction from the muscle of the castrated (C) and sham-operated (S) male AR-97Q mice, immunolabeled by N-20 (#7–8, 13-week-old). (C) Immunohistochemical study using 1C2 showed marked differences of diffuse nuclear staining and nuclear inclusions between the castrated and sham-operated AR-97Q mice in the spinal anterior horn and the muscle (#7–8, 13-week-old).

female AR-97Q mice exhibited motor weakness and dragged their hindlegs, which was not detected in the sesame oil-administered female AR-97Q mice (Figure 5F). Western blot analysis using N-20 revealed the mutant AR in the stacking gel in whole tissue homogenates as well as in the nuclear fraction, which was larger in amount in the testosterone-administered female AR-97Q mice than in the sesame oil-administered female AR-97Q mice (Figures 6A and 6B). The testosterone-administered female AR-97Q mice demonstrated markedly pronounced diffuse nuclear staining and NIs with 1C2 compared with the sesame oil-administered female AR-97Q mice (Figure 6C). The testosterone-administered female 97Q mice showed markedly higher serum testosterone levels (158.0 ± 70.7 ng/dl in #2–6, n = 3; 305.3 ± 182.3 ng/dl in #7–8, n = 4) than those in the sesame oil-administered female AR-97Q mice, all of which showed an undetectable low level.

Discussion

Our Tg mice with the full-length human *AR* containing 97 CAGs demonstrated progressive motor impairment and neuropathologic changes equivalent to human SBMA. Western blot analysis showed truncated fragments of mutant AR in the affected tissues. These fragments may contribute to pathophysiology in our Tg mice since several studies have suggested that proteolytic cleavage of mutant protein plays an important role in the pathogenic mechanisms of SBMA as well as other polyQ diseases (Li et al., 1998b; Kobayashi et al., 1998; Wellington et al., 1998; Mende-Mueller et al., 2001). Electron microscopic immunohistochemistry for 1C2 demonstrated granular aggregates and fine microaggregates, which indicates variable stages of pathologic change in the nucleus of motor neurons. Granular aggregate has also been reported in the pathologic study of

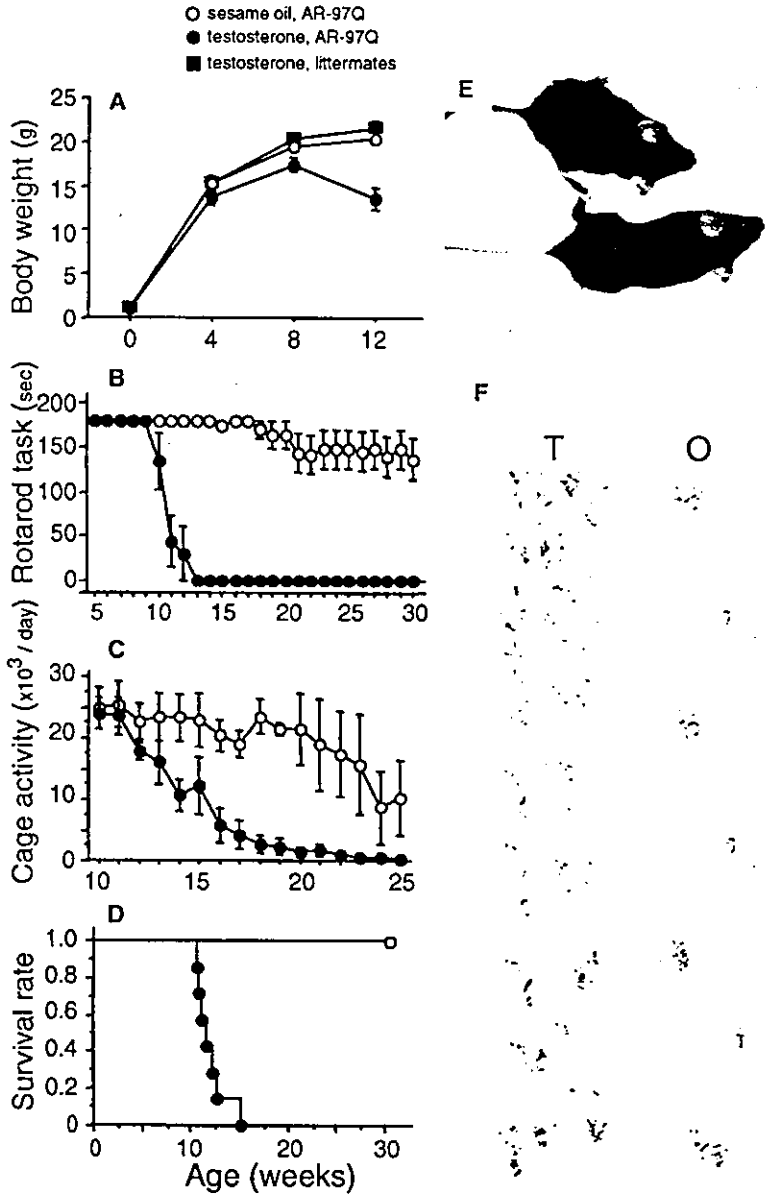

Figure 5. Effects of Testosterone Administration on the Symptomatic Phenotypes of Female AR-97Q Mice

(A–D) Body weight (A, #7–8), rotarod task (B, #7–8), cage activity (C, #2–6), and survival rate (D, #7–8) of the testosterone-administered (●, n = 7) and sesame oil-administered (○, n = 7) female AR-97Q mice. All parameters are significantly different between the testosterone-administered female AR-97Q mice and the sesame oil-administered female AR-97Q mice or testosterone-administered female littermates (■, n = 4) ($p < 0.0001$). (E) The testosterone-administered AR-97Q mouse (top) shows striking muscular atrophy, which is not demonstrated in the sesame oil-administered female AR-97Q mice (bottom) (#2–6, 14-week-old). (F) Footprints of 14-week-old testosterone-administered (T) and sesame oil-administered (O) female AR-97Q mice (#2–6).

SBMA (Li et al., 1998b). In our AR-97Q mice, neurogenic changes were evident in muscle pathology, and anterior horn cells and their axons showed significant decrease in size without substantial neuronal loss. These findings indicate that the main pathologic feature of our AR-97Q mice was neuronal dysfunction rather than degeneration of the spinal motor neurons, which was also demonstrated in a number of Tg mouse models of other polyQ diseases (Zoghbi and Orr, 2000; Rubinsztein, 2002). All symptomatic mice with AR-97Q showed motor impairment by 21 weeks of age; until this age, no lines with AR-24Q demonstrated rotarod deficit or weight loss in spite of the same expression levels of AR protein and similar copy numbers of the transgene. Nuclear inclusions and diffuse nuclear staining with 1C2 were found since 4 weeks of age even in female AR-97Q mice, although they are far less frequent than in male AR-97Q mice. Nevertheless, pathologic studies showed no abnormalities in AR-24Q mice at 12 weeks of age. These findings clarify that the symptomatic and pathologic phenotypes in AR-97Q were not due to overexpression of human AR but due to expanded polyglutamine tract. Moreover, no phenotypes were found in previous SBMA Tg mice with full-length human AR despite good transgene expression levels, presumably because the CAG repeat was not long enough (Bingham et al., 1995; La Spada et al., 1998).

Several Tg mouse models of SBMA have been reported so far. Since early models failed to manifest neurologic phenotypes (Bingham et al., 1995; La Spada et al., 1998; Merry et al., 1996), truncated AR and powerful promoter have been used in order to enhance phenotypes. A Tg mouse model of SBMA expressing expanded pure 239 CAGs under the control of human AR promoter (Adachi et al., 2001) and that carrying truncated *AR* with 112 CAGs controlled by prion protein

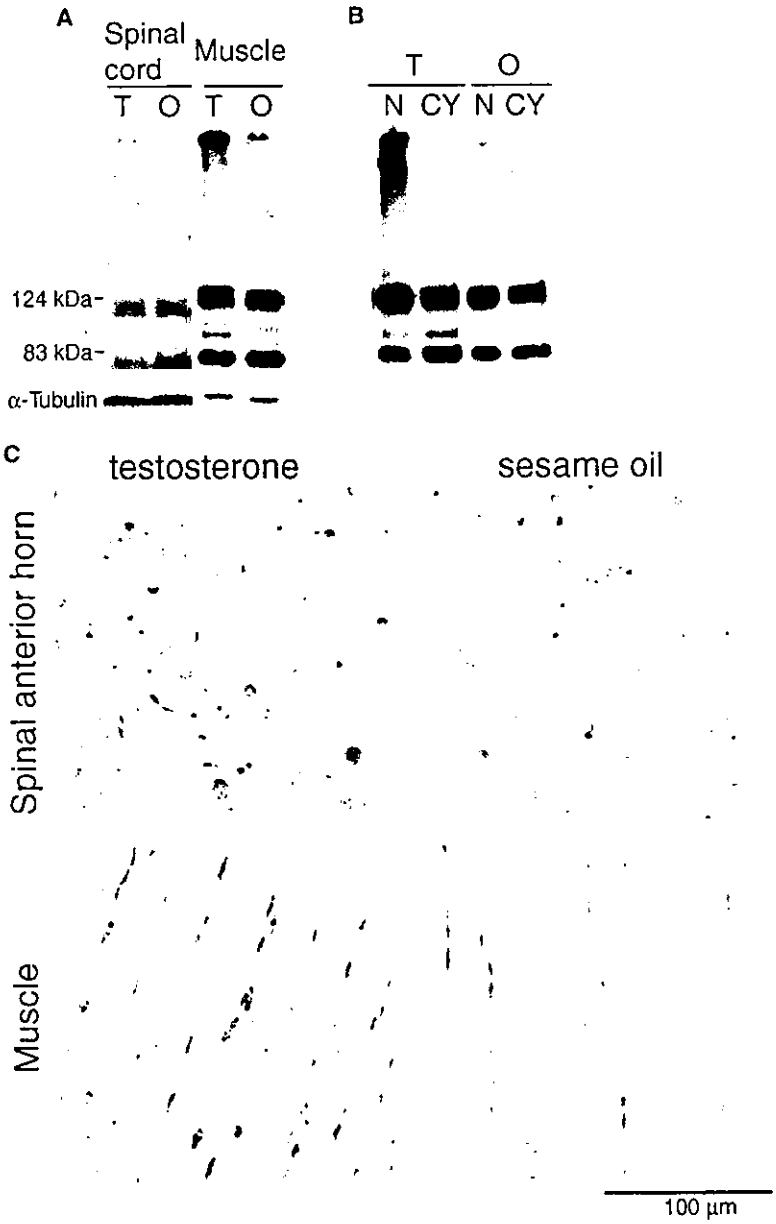

Figure 6. Effects of Testosterone Administration on Transgene Expression and Neuropathology of Female AR-97Q Mice

(A) Western blot analysis of total homogenates from the spinal cord and muscle of the testosterone-administered (T) and sesame oil-administered (O) female AR-97Q mice which were immunolabeled by N-20 (#2–6, 12-week-old). (B) Western blot analysis of nuclear (N) and cytoplasmic (CY) fraction from the muscle of the testosterone-administered (T) and sesame oil-administered (O) female AR-97Q mice, immunolabeled by N-20 (#2–6, 12-week-old). (C) Immunohistochemical study using 1C2 showed marked differences of diffuse nuclear staining and nuclear inclusions between the testosterone-administered and sesame oil-administered female AR-97Q mice in the spinal anterior horn and the muscle (#2–6, 12-week-old).

promoter (Abel et al., 2001) demonstrated progressive motor deficits and neuronal inclusions. They showed, however, no sexual difference of phenotypes because the transgenes of these Tg mice did not contain the ligand binding domain located in the C terminus of AR. Another Tg mouse model with the full-length AR showed motor impairment, although sexual difference of phenotypes has not been reported (Morrison et al., 2000).

The symptoms, pathologic findings, and nuclear localization of the mutant AR protein showed a remarkable sexual difference in our AR-97Q mice, and were significantly modified by hormonal intervention either by castration or testosterone administration. Although androgen has been shown to upregulate the expression of AR (Syms et al., 1985; Kemppainen et al., 1992; Zhou et al., 1995), RT-PCR did not reveal any significant sexual difference in the mRNA levels of the transgenic *AR* gene in our Tg mice, in which the transgene was not controlled by its own promoter with androgen-responsive element but by chicken β-actin promoter. These observations indicate that the testosterone level plays important roles in the sexual difference of phenotypes and effects of hormonal interventions, especially in the posttranscriptional stage of the mutant AR.

Castration dramatically prevented the phenotypic expression including neurologic findings in the male AR-97Q mice. The female AR-97Q mice, which showed few if any manifestations, demonstrated marked deterioration of symptoms by testosterone administration. The mutant AR located in the nuclei assessed by Western blot analysis and by immunohistochemistry with 1C2 dramatically diminished in the castrated male AR-97Q mice, and markedly increased in the testosterone-administered female AR-97Q mice. The castrated male AR-97Q

mice showed undetectable serum testosterone levels, whereas the testosterone-administered female AR-97Q mice showed markedly increased levels. Since the nuclear translocation of AR is solely dependent on testosterone (Stenoien et al., 1999; Simeoni et al., 2000), testosterone may show toxic effects in the female AR-97Q mice by accelerating nuclear translocation of the mutant AR. By contrast, castration prevented the nuclear localization of the mutant AR by reducing the testosterone level. The nuclear localization of the mutant protein with expanded polyQ is important in inducing neuronal cell dysfunction and degeneration in the majority of polyQ diseases. Addition of a nuclear export signal to the mutant huntingtin eliminates aggregate formation and cell death in cell models of HD (Saudou et al., 1998; Peters et al., 1999), and a nuclear localization signal had the opposite effect (Peters et al., 1999). In Tg mice of SCA1 having a mutated nuclear localization signal, ataxin-1 was distributed in the cytoplasm, and the mice did not show any neurologic disorders (Klement et al., 1998). These findings suggest that reduction of testosterone ameliorates phenotypic expression by preventing nuclear localization of the mutant AR. We emphasize that our approach, hormonal intervention to diminish testosterone level, can be applied to human therapy.

The castrated AR-97Q mice showed phenotypes similar to those of the female AR-97Q mice, implying that motor impairment of SBMA patients can be rescued to the level in female carriers. Almost half of the human SBMA female carriers showed mild subclinical electromyographic abnormalities, while few manifested clinical phenotypes (Sobue et al., 1993; Mariotti et al., 2000). Indeed, lower expression level of mutant AR in female carriers due to X inactivation may cause the escape from the manifestation, but our present study also suggests that the low level of testosterone prevents the nuclear localization of the expressed mutant AR, resulting in a lack of phenotypic manifestations in the female carriers.

A toxic gain of function has been considered the main stream of the pathophysiology in polyQ diseases, but a loss of function of mutant proteins may also play a role (Zoghbi and Orr, 2000; Rubinsztein, 2002). Although the expansion of polyQ tract in AR deteriorates the transcriptional activities of AR, and affects its interaction with other transcriptional factors and activators (Mhatre et al., 1993; Kazemi-Esfarjani et al., 1995; Chamberlain et al., 1994; Nakajima et al., 1996), the neurologic impairment in SBMA cannot be attributed to the loss of AR function (Maclean et al., 1995; McPhaul et al., 1993), a reason why testosterone shows insufficient and transient effects when used as a therapeutic agent for SBMA (Danek et al., 1994; Goldenberg and Bradley, 1996; Neuschmid-Kaspar et al., 1996). The present study further suggests that the major pathogenic mechanism of SBMA is a toxic gain of function of mutant AR with expanded polyQ, particularly when located in the nuclei. Although molecular mechanisms still remain to be elucidated, several studies have revealed that nuclear accumulation of the mutant protein resulted in sequestration of transcriptional regulatory proteins in SBMA and other polyQ diseases (McCampbell et al., 2000; Steffan et al., 2000; Nucifora et al., 2001).

There have been no substantially effective therapeutic approaches to the polyQ diseases. In a Tg mouse model of HD, expression of a dominant-negative caspase-1 mutant extended survival and delayed the appearance of neuronal inclusions, neurotransmitter receptor alterations, and onset of symptoms (Ona et al., 1999). Inhibition of mutant gene expression demonstrated the reversibility of phenotypic progression in a Tg mouse model of HD (Yamamoto et al., 2000). However, these gene modulations cannot be directly applied clinically. Transglutaminase inhibitors suppressed aggregate formation and apoptosis in a cell model of DRPLA (Igarashi et al., 1998) and prolonged survival in a Tg mouse model of HD (Karpuj et al., 2002). An in vitro model of HD showed inhibition of huntingtin fibrillogenesis by specific antibodies and small molecules (Heiser et al., 2000). Creatine increased survival and delayed motor symptoms in a Tg mouse model of HD (Andreassen et al., 2001). Overexpression of molecular chaperone HSP70 demonstrated preventive effects in a *Drosophila* model of Machado-Joseph disease (Warrick et al., 1999) and SCA1 cell and Tg mouse models (Cummings et al., 1998, 2001). HSP70 and HSP40 showed preventive effects also in an SBMA cell model (Kobayashi et al., 2000). These and other therapeutic approaches have, yet, remained insufficient or minimal in prevention of phenotypic expression and progression. Recently reported histone deacetylase inhibitors in a *Drosophila* model could be a promising candidate therapy for polyQ diseases (Steffan et al., 2001), but their therapeutic efficacy should be assessed in a Tg mouse model. Although no specific ligand of the mutant protein has been revealed in other polyQ diseases, the striking therapeutic effects of castration in our Tg mice further suggests that patients with polyQ disease can be rescued by prevention of the nuclear translocation of the mutant proteins. We emphasize that it is necessary to investigate hormone-like small molecules which alter the nuclear localization of mutant proteins for therapy of polyQ diseases.

Experimental Procedures

Transgene Construction

Chicken β-actin promoter-driven AR-24Q and AR-97Q constructs were prepared by digestion of pCAGGS vector (Niwa et al., 1991) by HindIII and ligation after filling in, which generated the new NheI site (pCAGGS-NheI). The full-length human *AR* fragment harboring 24 or 97 CAGs (Kobayashi et al., 1998) was subcloned into pCAGGS-NheI. By direct DNA sequencing, the presence of 24 and 97 CAG repeat sequences was confirmed in the 5.3 and 5.5 kb inserts, respectively.

Generation and Maintenance of Tg Mice and Genotyping

The final plasmids with SalI-NheI were digested to remove the *AR* fragments. We generated Tg mice by microinjection into BDF1 fertilized eggs, and obtained three founders with AR-24Q and five founders with AR-97Q. These mice were backcrossed to C57BL/6J. We screened mouse tail DNA by PCR for the presence of the transgene using the primers 5′-CTTCTGGCGTGTGACCGGCG -3′ and 5′-TGAGCTTGG CTGAATCTTCC-3′ and the confirmation of the CAG repeat size using the primers 5′-CCAGAGCGTGCGCGAAGTG-3′ and 5′-TGTGA AGGTTGCTGTTCCTC-3′. The transgene copy number in each line was determined by densitometric comparison of Southern blot hybridization intensity of the *AR* DNA with known standards cutting only one site in the transgene using SacII. For determining CAG repeat size, we electrophoresed the PCR products amplified with a Texas Red-labeled primer on 6% denaturing polyacrylamide gel for 12 hr using a 5500 DNA sequencer (Hitachi, Tokyo, Japan).

Neurological and Behavioral Testing

We analyzed rotarod task of mice by an Economex Rotarod (Columbus Instruments, Colombus, Ohio) weekly during the light phase of the 12 hr light/12 hr dark cycle as described previously (Adachi et al., 2001). We performed three trials, and recorded the longest duration on the rod for every mouse. We stopped the timer when the mouse fell from the rod or after an arbitrary limit of 180 s.

We measured cage activity while each mouse was in a transparent acrylic cage (16 × 30 × 14 cm, width × depth × height) housed in a soundproofed box. We used an AB system (Neuroscience, Tokyo, Japan) with an infrared ray sensor monitor to measure spontaneous motor activity. We automatically totaled and recorded all measurements for 24 hr per week at 10 min intervals.

Hormonal Intervention and Serum Testosterone Assay

Male AR-97Q mice and their normal littermates were castrated or sham-operated via the abdominal route under ketamine-xylazine anesthesia (50 mg/kg ketamine and 10 mg/kg xylazine, i.p.) at 4 weeks of age. Female AR-97Q mice and their littermates were subcutaneously injected 20 μg of testosterone enanthate dissolved in 20 μl of sesame oil weekly from 4 weeks of age until the end of the analysis. The sesame oil-administered mice were given the same amount of sesame oil.

We used Coat-A-Count Total Testosterone radioimmunoassay (Diagnostic Products Corporation, Los Angeles, California) for assaying the serum testosterone levels.

RNA and Protein Expression Analysis

We exsanguinated mice under ketamine-xylazine anesthesia, snap-froze their tissues with powdered CO_2 in acetone, extracted total RNA from tissues with Trizol (Life Technologies/Gibco BRL, Gaithersburg, Maryland), and reverse transcribed the RNA using SUPERSCRIPT II reverse transcriptase (Life Technologies/Gibco BRL). We used 5′-TTCCACACCCAGTGAAGC-3′ and 5′-GGCATTGGCCACAC CAAGCC-3′ as primers for specific transgene RNA detection. After amplification, the products were separated by agarose gel electrophoresis. We compared the intensity of the PCR products signals with those of β-actin mRNA levels, which were separately amplified, by ethidium bromide staining.

Frozen tissue (0.1 g wet weight) was homogenized in 1000 μl of 50 mM Tris (pH 8.0), 150 mM NaCl, 1% NP-40, 0.5% deoxycholate, 0.1% SDS, and 1 mM 2-mercaptoethanol with 1 mM PMSF and aprotinine at 6 μg/ml (2500 g for 15 min at 4°C). Each lane on a 5%–20% SDS-PAGE gel was loaded with protein 200 μg for nervous tissue, and 80 μg for muscular tissue from the supernatant fraction, which was transferred to Hybond-P membranes (Amersham Pharmacia Biotech, Buckinghamshire, England), using 25 mM Tris, 192 mM glycine, 0.1% SDS, and 10% methanol as transfer buffer. After immunoprobing with rabbit anti-AR antibody N-20 (1:1000) (Santa Cruz Biotechnology, Santa Cruz, California), we performed second antibody probing and detection using the ECL+plus kit (Amersham Pharmacia Biotech). Nuclear and cytoplasmic fractions were extracted with NE-PER nuclear and cytoplasmic extraction reagents (Pierce, Rockford, Illinois).

Immunohistochemistry

We perfused 20 ml of a 4% paraformaldehyde fixative in phosphate buffer (pH 7.4) through the left cardiac ventricle of mice deeply anesthetized with ketamine-xylazine, postfixed tissues overnight in 10% phosphate-buffered formalin, and processed tissues for paraffin embedding. Then we deparaffinized 4 μm thick tissue sections, dehydrated with alcohol, treated in formic acid for 5 min at room temperature, and stained with 1C2 (1:10000) (Chemicon, Temecula, California), as described before (Adachi et al., 2001).

For electron microscopic immunohistochemistry, we used paraffin-embedded tissue sections immunostained with 1C2 (1:10000) (Chemicon) as described previously (Adachi et al., 2001).

Muscle Histology and Morphometric Analysis of Spinal Motor Neurons and Ventral Spinal Roots

Six micrometer thick cryostat sections of the gastrocnemius muscles were air dried and stained with hematoxylin and eosin (H & E).

For assessment of the neuronal populations and cross-sectional area of the anterior horn cells, 20 serial 5 μm thick sections from the fifth lumbar spinal cords of three mice of each group (#7–8, 13-week-old) were prepared. Every other section was stained by the Nissl technique and all neurons with an obvious nucleolus, present in the anterior horn, were assessed using a Luzex FS image analyzer (Nireco, Tokyo, Japan) as described before (Terao et al., 1996). The diameter of myelinated fibers in the ventral spinal roots was measured on the transverse sections stained with toluidine blue as described before (Terao et al., 1996).

Statistical Analysis

We analyzed data using the unpaired t test and denoted p values of 0.05 or less as statistical significance.

Acknowledgments

We thank Dr. Jun-ichi Miyazaki for kindly providing pCAGGS vector, Dr. Masahiko Nishimura and Dr. Azumi Wada for instruction of castration, and Dr. Takashi Osada for preparation of testosterone. This work was supported by a Center-of-Excellence (COE) grant from the Ministry of Education, Culture, Sports, Science and Technology, Japan and grants from the Ministry of Health, Labor and Welfare, Japan.

Received: December 27, 2001
Revised: July 8, 2002

References

Abel, A., Walcott, J., Woods, J., Duda, J., and Merry, D.E. (2001). Expression of expanded repeat androgen receptor produces neurologic disease in transgenic mice. Hum. Mol. Genet. *10*, 107–116.

Adachi, H., Kume, A., Li, M., Nakagomi, Y., Niwa, H., Do, J., Sang, C., Kobayashi, Y., Doyu, M., and Sobue, G. (2001). Transgenic mice with an expanded CAG repeat controlled by the human AR promoter show polyglutamine nuclear inclusions and neuronal dysfunction without neuronal cell death. Hum. Mol. Genet. *10*, 1039–1048.

Andreassen, O.A., Dedeoglu, A., Ferrante, R.J., Jenkins, B.G., Ferrante, K.L., Thomas, M., Friedlich, A., Browne, S.E., Schilling, G., Borchelt, D.R., et al. (2001). Creatine increases survival and delays motor symptoms in a transgenic animal model of Huntington's disease. Neurobiol. Dis. *8*, 479–491.

Bingham, P.M., Scott, M.O., Wang, S., McPhaul, M.J., Wilson, E.M., Garbern, J.Y., Merry, D.E., and Fischbeck, K.H. (1995). Stability of an expanded trinucleotide repeat in the androgen receptor gene in transgenic mice. Nat. Genet. *9*, 191–196.

Chamberlain, N.L., Driver, E.D., and Miesfeld, R.L. (1994). The length and location of CAG trinucleotide repeats in the androgen receptor N-terminal domain affect transactivation function. Nucleic Acids Res. *22*, 3181–3186.

Cummings, C.J., Mancini, M.A., Antalffy, B., DeFranco, D.B., Orr, H.T., and Zoghbi, H.Y. (1998). Chaperone suppression of aggregation and altered subcellular proteasome localization imply protein misfolding in SCA1. Nat. Genet. *19*, 148–154.

Cummings, C.J., Reinstein, E., Sun, Y., Antalffy, B., Jiang, Y., Ciechanover, A., Orr, H.T., Beaudet, A.L., and Zoghbi, H.Y. (1999). Mutation of the E6-AP ubiquitin ligase reduces nuclear inclusion frequency while accelerating polyglutamine-induced pathology in SCA1 mice. Neuron *24*, 879–892.

Cummings, C.J., Sun, Y., Opal, P., Antalffy, B., Mestril, R., Orr, H.T., Dillmann, W.H., and Zoghbi, H.Y. (2001). Over-expression of inducible HSP70 chaperone suppresses neuropathology and improves motor function in SCA1 mice. Hum. Mol. Genet. *10*, 1511–1518.

Danek, A., Witt, T.N., Mann, K., Schweikert, H.U., Romalo, G., La Spada, A.R., and Fischbeck, K.H. (1994). Decrease in androgen binding and effect of androgen treatment in a case of X-linked bulbospinal neuronopathy. Clin. Investig. *72*, 892–897.

Duyao, M., Ambrose, C., Myers, R., Novelletto, A., Persichetti, F., Frontali, M., Folstein, S., Ross, C., Franz, M., Abbott, M., et al. (1993). Trinucleotide repeat length instability and age of onset in Huntington's disease. Nat. Genet. *4*, 387–392.

Doyu, M., Sobue, G., Mukai, E., Kachi, T., Yasuda, T., Mitsuma, T., and Takahashi, A. (1992). Severity of X-linked recessive bulbospinal neuronopathy correlates with size of the tandem CAG repeat in androgen receptor gene. Ann. Neurol. *32*, 707–710.

Goldenberg, J.N., and Bradley, W.G. (1996). Testosterone therapy and the pathogenesis of Kennedy's disease (X-linked bulbospinal muscular atrophy). J. Neurol. Sci. *135*, 158–161.

Gutekunst, C.A., Li, S.H., Yi, H., Mulroy, J.S., Kuemmerle, S., Jones, R., Rye, D., Ferrante, R.J., Hersch, S.M., and Li, X.J. (1999). Nuclear and neuropil aggregates in Huntington's disease: relationship to neuropathology. J. Neurosci. *19*, 2522–2534.

Heiser, V., Scherzinger, E., Boeddrich, A., Nordhoff, E., Lurz, R., Schugardt, N., Lehrach, H., and Wanker, E.E. (2000). Inhibition of huntingtin fibrillogenesis by specific antibodies and small molecules: implications for Huntington's disease therapy. Proc. Natl. Acad. Sci. USA *97*, 6739–6744.

Igarashi, S., Tanno, Y., Onodera, O., Yamazaki, M., Sato, S., Ishikawa, A., Miyatani, N., Nagashima, M., Ishikawa, Y., Sahashi, K., et al. (1992). Strong correlation between the number of CAG repeats in androgen receptor genes and the clinical onset of features of spinal and bulbar muscular atrophy. Neurology *42*, 2300–2302.

Igarashi, S., Koide, R., Shimohata, T., Yamada, M., Hayashi, Y., Takano, H., Date, H., Oyake, M., Sato, T., Sato, A., et al. (1998). Suppression of aggregate formation and apoptosis by transglutaminase inhibitors in cells expressing truncated DRPLA protein with an expanded polyglutamine stretch. Nat. Genet. *18*, 111–117.

Karpuj, M.V., Becher, M.W., Springer, J.E., Chabas, D., Youssef, S., Pedotti, R., Mitchell, D., and Steinman, L. (2002). Prolonged survival and decreased abnormal movements in transgenic model of Huntington disease, with administration of the transglutaminase inhibitor cystamine. Nat. Med. *8*, 143–149.

Kazemi-Esfarjani, P., Trifiro, M.A., and Pinsky, L. (1995). Evidence for a repressive function of the long polyglutamine tract in the human androgen receptor: possible pathogenetic relevance for the (CAG)n-expanded neuronopathies. Hum. Mol. Genet. *4*, 523–527.

Kemppainen, J.A., Lane, M.V., Sar, M., and Wilson, E.M. (1992). Androgen receptor phosphorylation, turnover, nuclear transport and transcriptional activation. J. Biol. Chem. *267*, 968–974.

Kennedy, W.R., Alter, M., and Sung, J.H. (1968). Progressive proximal spinal and bulbar muscular atrophy of late onset. A sex-linked recessive trait. Neurology *18*, 671–680.

Klement, I.A., Skinner, P.J., Kaytor, M.D., Yi, H., Hersch, S.M., Clark, H.B., Zoghbi, H.Y., and Orr, H.T. (1998). Ataxin-1 nuclear localization and aggregation: role in polyglutamine-induced disease in SCA1 transgenic mice. Cell *95*, 41–53.

Kobayashi, Y., Miwa, S., Merry, D.E., Kume, A., Mei, L., Doyu, M., and Sobue, G. (1998). Caspase-3 cleaves the expanded androgen receptor protein of spinal and bulbar muscular atrophy in a polyglutamine repeat length-dependent manner. Biochem. Biophys. Res. Commun. *252*, 145–150.

Kobayashi, Y., Kume, A., Li, M., Doyu, M., Hata, M., Ohtsuka, K., and Sobue, G. (2000). Chaperones Hsp70 and Hsp40 suppress aggregate formation and apoptosis in cultured neuronal cells expressing truncated androgen receptor protein with expanded polyglutamine tract. J. Biol. Chem. *275*, 8772–8778.

La Spada, A.R., Wilson, E.M., Lubahn, D.B., Harding, A.E., and Fischbeck, K.H. (1991). Androgen receptor gene mutations in X-linked spinal and bulbar muscular atrophy. Nature *352*, 77–79.

La Spada, A.R., Roling, D.B., Harding, A.E., Warner, C.L., Spiegel, R., Hausmanowa-Petrusewicz, I., Yee, W.C., and Fischbeck, K.H. (1992). Meiotic stability and genotype-phenotype correlation of the trinucleotide repeat in X-linked spinal and bulbar muscular atrophy. Nat. Genet. *2*, 301–304.

La Spada, A.R., Peterson, K.R., Meadows, S.A., McClain, M.E., Jeng, G., Chmelar, R.S., Haugen, H.A., Chen, K., Singer, M.J., Moore, D., et al. (1998). Androgen receptor YAC transgenic mice carrying CAG 45 alleles show trinucleotide repeat instability. Hum. Mol. Genet. *7*, 959–967.

Li, M., Miwa, S., Kobayashi, Y., Merry, D.E., Yamamoto, M., Tanaka, F., Doyu, M., Hashizume, Y., Fischbeck, K.H., and Sobue, G. (1998a). Nuclear inclusions of the androgen receptor protein in spinal and bulbar muscular atrophy. Ann. Neurol. *44*, 249–254.

Li, M., Nakagomi, Y., Kobayashi, Y., Merry, D.E., Tanaka, F., Doyu, M., Mitsuma, T., Hashizume, Y., Fischbeck, K.H., and Sobue, G. (1998b). Nonneural nuclear inclusions of androgen receptor protein in spinal and bulbar muscular atrophy. Am. J. Pathol. *153*, 695–701.

MacLean, H.E., Warne, G.L., and Zajac, J.D. (1995). Defects of androgen receptor function: from sex reversal to motor neurone disease. Mol. Cell. Endocrinol. *112*, 133–141.

Mariotti, C., Castellotti, B., Pareyson, D., Testa, D., Eoli, M., Antozzi, C., Silani, V., Marconi, R., Tezzon, F., Siciliano, G., et al. (2000). Phenotypic manifestations associated with CAG-repeat expansion in the androgen receptor gene in male patients and heterozygous females: a clinical and molecular study of 30 families. Neuromuscul. Disord. *10*, 391–397.

McCampbell, A., Taylor, J.P., Taye, A.A., Robitschek, J., Li, M., Walcott, J., Merry, D., Chai, Y., Paulson, H., Sobue, G., and Fischbeck, K.H. (2000). CREB-binding protein sequestration by expanded polyglutamine. Hum. Mol. Genet. *9*, 2197–2202.

McPhaul, M.J., Marcelli, M., Zoppi, S., Griffin, J.E., and Wilson, J.D. (1993). Genetic basis of endocrine disease. 4. The spectrum of mutations in the androgen receptor gene that causes androgen resistance. J. Clin. Endocrinol. Metab. *76*, 17–23.

Mende-Mueller, L.M., Toneff, T., Hwang, S.R., Chesselet, M.F., and Hook, V.Y. (2001). Tissue-specific proteolysis of Huntingtin (htt) in human brain: evidence of enhanced levels of N- and C-terminal htt fragments in Huntington's disease striatum. J. Neurosci. *21*, 1830–1837.

Merry, D.E., McCampbell, A., Taye, A.A., Winston, R.L., and Fischbeck, K.H. (1996). Toward a mouse model for spinal and bulbar muscular atrophy: effect of neuronal expression of androgen receptor in transgenic mice. Am. J. Hum. Genet. Suppl. *59*, A271.

Mhatre, A.N., Trifiro, M.A., Kaufman, M., Kazemi-Esfarjani, P., Figlewicz, D., Rouleau, G., and Pinsky, L. (1993). Reduced transcriptional regulatory competence of the androgen receptor in X-linked spinal and bulbar muscular atrophy. Nat. Genet. *5*, 184–188.

Morrison, J.P., McManamny, P., O'Bryan, K.M., Cimdins, K.L., Kola, I., Cheema, S., and deKretser, D.M. (2000). A mouse model of spinal bulbar muscular atrophy (SBMA). Am. J. Hum. Genet. Suppl. *67*, A51.

Nakajima, H., Kimura, F., Nakagawa, T., Furutama, D., Shinoda, K., Shimizu, A., and Ohsawa, N. (1996). Transcriptional activation by the androgen receptor in X-linked spinal and bulbar muscular atrophy. J. Neurol. Sci. *142*, 12–16.

Neuschmid-Kaspar, F., Gast, A., Peterziel, H., Schneikert, J., Mulgg, A., Ransmayr, G., Klocker, H., Bartsch, G., and Cato, A.C. (1996). CAG-repeat expansion in androgen receptor in Kennedy's disease is not a loss of function mutation. Mol. Cell. Endocrinol. *117*, 149–156.

Niwa, H., Yamamura, K., and Miyazaki, J. (1991). Efficient selection for high-expression transfectants with a novel eukaryotic vector. Gene *108*, 193–199.

Nucifora, F.C., Jr., Sasaki, M., Peters, M.F., Huang, H., Cooper, J.K., Yamada, M., Takahashi, H., Tsuji, S., Troncoso, J., Dawson, V.L., et al. (2001). Interference by huntingtin and atrophin-1 with CBP-mediated transcription leading to cellular toxicity. Science *291*, 2423–2428.

Ona, V.O., Li, M., Vonsattel, J.P., Andrews, L.J., Khan, S.Q., Chung, W.M., Frey, A.S., Menon, A.S., Li, X.J., Stieg, P.E., et al. (1999). Inhibition of caspase-1 slows disease progression in a mouse model of Huntington's disease. Nature *399*, 263–267.

Orr, H.T., Chung, M.Y., Banfi, S., Kwiatkowski, T.J., Jr., Servadio, A., Beaudet, A.L., McCall, A.E., Duvick, L.A., Ranum, L.P., and Zoghbi, H.Y. (1993). Expansion of an unstable trinucleotide CAG repeat in spinocerebellar ataxia type 1. Nat. Genet. *4*, 221–226.

Paulson, H.L. (2000). Toward an understanding of polyglutamine neurodegeneration. Brain Pathol. *10*, 293–299.

Peters, M.F., Nucifora, F.C., Jr., Kushi, J., Seaman, H.C., Cooper, J.K., Herring, W.J., Dawson, V.L., Dawson, T.M., and Ross, C.A.

(1999). Nuclear targeting of mutant Huntingtin increases toxicity. Mol. Cell. Neurosci. *14*, 121–128.

Rubinsztein, D.C. (2002). Lessons from animal models of Huntington's disease. Trends Genet. *18*, 202–209.

Saudou, F., Finkbeiner, S., Devys, D., and Greenberg, M.E. (1998). Huntingtin acts in the nucleus to induce apoptosis but death does not correlate with the formation of intranuclear inclusions. Cell *95*, 55–66.

Simeoni, S., Mancini, M.A., Stenoien, D.L., Marcelli, M., Weigel, N.L., Zanisi, M., Martini, L., and Poletti, A. (2000). Motoneuronal cell death is not correlated with aggregate formation of androgen receptors containing an elongated polyglutamine tract. Hum. Mol. Genet. *9*, 133–144.

Sobue, G., Hashizume, Y., Mukai, E., Hirayama, M., Mitsuma, T., and Takahashi, A. (1989). X-linked recessive bulbospinal neuronopathy. A clinicopathological study. Brain *112*, 209–232.

Sobue, G., Doyu, M., Kachi, T., Yasuda, T., Mukai, E., Kumagai, T., and Mitsuma, T. (1993). Subclinical phenotypic expressions in heterozygous females of X-linked recessive bulbospinal neuronopathy. J. Neurol. Sci. *117*, 74–78.

Steffan, J.S., Kazantsev, A., Spasic-Boskovic, O., Greenwald, M., Zhu, Y.Z., Gohler, H., Wanker, E.E., Bates, G.P., Housman, D.E., and Thompson, L.M. (2000). The Huntington's disease protein interacts with p53 and CREB-binding protein and represses transcription. Proc. Natl. Acad. Sci. USA *97*, 6763–6768.

Steffan, J.S., Bodai, L., Pallos, J., Poelman, M., McCampbell, A., Apostol, B.L., Kazantsev, A., Schmidt, E., Zhu, Y.Z., Greenwald, M., et al. (2001). Histone deacetylase inhibitors arrest polyglutamine-dependent neurodegeneration in Drosophila. Nature *413*, 739–743.

Stenoien, D.L., Cummings, C.J., Adams, H.P., Mancini, M.G., Patel, K., DeMartino, G.N., Marcelli, M., Weigel, N.L., and Mancini, M.A. (1999). Polyglutamine-expanded androgen receptors form aggregates that sequester heat shock proteins, proteasome components and SRC-1, and are suppressed by the HDJ-2 chaperone. Hum. Mol. Genet. *8*, 731–741.

Syms, A.J., Norris, J.S., Panko, W.B., and Smith, R.G. (1985). Mechanism of androgen-receptor augmentation: analysis of receptor synthesis and degradation by the density-shift technique. J. Biol. Chem. *260*, 455–461.

Tanaka, F., Reeves, M.F., Ito, Y., Matsumoto, M., Li, M., Miwa, S., Inukai, A., Yamamoto, M., Doyu, M., Yoshida, M., et al. (1999). Tissue-specific somatic mosaicism in spinal and bulbar muscular atrophy is dependent on CAG-repeat length and androgen receptor-gene expression level. Am. J. Hum. Genet. *65*, 968–973.

Terao, S., Sobue, G., Hashizume, Y., Li, M., Inagaki, T., and Mitsuma, T. (1996). Age-related changes in human spinal ventral horn cells with special reference to the loss of small neurons in the intermediate zone: a quantitative analysis. Acta Neuropathol. (Berl.) *92*, 109–114.

Trottier, Y., Lutz, Y., Stevanin, G., Imbert, G., Devys, D., Cancel, G., Saudou, F., Weber, C., David, G., Tora, L., et al. (1995). Polyglutamine expansion as a pathological epitope in Huntington's disease and four dominant cerebellar ataxias. Nature *378*, 403–406.

Warrick, J.M., Chan, H.Y., Gray-Board, G.L., Chai, Y., Paulson, H.L., and Bonini, N.M. (1999). Suppression of polyglutamine-mediated neurodegeneration in Drosophila by the molecular chaperone HSP70. Nat. Genet. *23*, 425–428.

Wellington, C.L., Ellerby, L.M., Hackam, A.S., Margolis, R.L., Trifiro, M.A., Singaraja, R., McCutcheon, K., Salvesen, G.S., Propp, S.S., Bromm, M., et al. (1998). Caspase cleavage of gene products associated with triplet expansion disorders generates truncated fragments containing the polyglutamine tract. J. Biol. Chem. *273*, 9158–9167.

Yamamoto, A., Lucas, J.J., and Hen, R. (2000). Reversal of neuropathology and motor dysfunction in a conditional model of Huntington's disease. Cell *101*, 57–66.

Zhou, Z.X., Wong, C.I., Sar, M., and Wilson, E.M. (1994). The androgen receptor: an overview. Recent Prog. Horm. Res. *49*, 249–274.

Zhou, Z.X., Lane, M.V., Kemppainen, J.A., French, F.S., and Wilson, E.M. (1995). Specificity of ligand-dependent androgen receptor stabilization: receptor domain interactions influence ligand dissociation and receptor stability. Mol. Endocrinol. *9*, 208–218.

Zoghbi, H.Y., and Orr, H.T. (2000). Glutamine repeats and neurodegeneration. Annu. Rev. Neurosci. *23*, 217–247.

THE JOURNAL OF BIOLOGICAL CHEMISTRY
Vol. 277, No. 52, Issue of December 27, pp. 50966–50972, 2002
Printed in U.S.A.

Mitochondrial Localization of Mutant Superoxide Dismutase 1 Triggers Caspase-dependent Cell Death in a Cellular Model of Familial Amyotrophic Lateral Sclerosis*

Received for publication, September 12, 2002
Published, JBC Papers in Press, October 21, 2002, DOI 10.1074/jbc.M209356200

Hideyuki Takeuchi, Yasushi Kobayashi, Shinsuke Ishigaki, Manabu Doyu, and Gen Sobue‡

From the Department of Neurology, Nagoya University Graduate School of Medicine, 65 Tsurumai-cho, Showa-ku, Nagoya 466-8550, Japan

The mutations in superoxide dismutase 1 (SOD1) cause ~20% of familial amyotrophic lateral sclerosis cases. A toxic gain of function has been considered to be the cause of the disease, but its molecular mechanism remains uncertain. To determine whether the subcellular localization of mutant SOD1 is crucial to mutant SOD1-mediated cell death, we produced neuronal cell models with accumulation of SOD1 in each subcellular fraction/organelle, such as the cytosol, nucleus, endoplasmic reticulum, and mitochondria. We showed that the localization of mutant SOD1 in the mitochondria triggered the release of mitochondrial cytochrome *c* followed by the activation of caspase cascade and induced neuronal cell death without cytoplasmic mutant SOD1 aggregate formation. Nuclear and endoplasmic reticulum localization of mutant SOD1 did not induce cell death. These results suggest that the localization of mutant SOD1 in the mitochondria is critical in the pathogenesis of mutant SOD1-associated familial amyotrophic lateral sclerosis.

Amyotrophic lateral sclerosis (ALS)[1] is a paralytic and lethal disease caused by selective death of motor neurons. Approximately 10% of ALS cases occur in familial (FALS) form. The mutations in superoxide dismutase 1 (SOD1) cause ~20% of FALS cases (1, 2), and there is overwhelming evidence of a toxic gain of function as the cause of the disease (3, 4). However, it remains unclear how mutant SOD1 causes the cell death of motor neurons.

Mitochondrial degeneration such as swelling, dilatation, and vacuolation and cytoplasmic aggregate formation containing mutant SOD1 are characteristic pathological features of FALS cases and FALS transgenic mice models with SOD1 mutations (2, 4–9). The major question is where and how mutant SOD1 exerts its toxic function in motor neuron degeneration. In polyglutamine diseases, nuclear localization of mutant proteins with expanded polyglutamine tract is considered an essential process in causing neuronal cell death (10–14). Endoplasmic reticulum (ER) stress by unfolded protein accumulation in the ER is considered to cause familial Alzheimer's disease (15, 16) or autosomal recessive juvenile Parkinsonism (17). These reports suggest that the subcellular localization of mutant or modified protein is crucial to neuronal cell degeneration. In mutant SOD1-associated FALS, many reports have documented that the mitochondria is involved in the pathogenic process (18–26). Moreover, it has been demonstrated that SOD1, considered a cytosolic enzyme, exists in the mitochondria (27–29), suggesting that the mitochondria is the important site in pathogenesis of FALS. On the other hand, it remains controversial as to whether cytoplasmic mutant SOD1 aggregates are toxic (30) or not (31–33). Previous studies have demonstrated that the inhibition of cytoplasmic aggregate formation by heat shock proteins assure cell survival at an early stage but is unable to prevent eventual cell death at the late stage in the *in vitro* models of FALS (34, 35). Thus, it is important to determine in which organelle of the neuron mutant SOD1 triggers neuronal cell death. To examine this issue, we have produced neuronal cell models with the obligatory accumulation of SOD1 in the subcellular fraction/organelle of the cytosol, nucleus, ER, and mitochondria. In the present study, we provided unequivocal evidence that localization of mutant SOD1 in the mitochondria is the primary cause of mutant SOD1-mediated neuronal cell death, triggering the release of mitochondrial cytochrome *c* followed by the activation of caspase cascade. Furthermore, we demonstrated that cytoplasmic mutant SOD1 aggregate formation is independent of mutant SOD1-mediated neuronal cell death.

EXPERIMENTAL PROCEDURES

Plasmid Constructs—The non-organelle-oriented vectors expressing the fusion proteins of human SOD1 (wild type, mutant G93A, and G85R) and enhanced green fluorescent protein (EGFP) were generated with pEGFP-N1 vector (Clontech) as described previously (35). These vectors were designated Cyto-wtSOD1, Cyto-mSOD1^{G93A}, and Cyto-mSOD1^{G85R}, respectively. After these constructs were digested with *Xho*I and *Not*I, EGFP-tagged human SOD1 (wild type, mutant G93A, and G85R) was subcloned into the *Xho*I/*Not*I site of pShooter vectors (pCMV/myc/nuc, pCMV/myc/ER, and pCMV/myc/mito; Invitrogen). The nucleus-oriented vectors with nuclear localizing signals were designated Nuc-wtSOD1, Nuc-mSOD1^{G93A}, and Nuc-mSOD1^{G85R}, respectively. The ER-oriented vectors with ER retention signals were designated ER-wtSOD1, ER-mSOD1^{G93A}, and ER-mSOD1^{G85R}, respectively. The mitochondria-oriented vectors with mitochondrial localizing signals were designated Mito-wtSOD1, Mito-mSOD1^{G93A}, and Mito-mSOD1^{G85R}, respectively. As controls, we used LacZ subcloned into pEGFP-N1 vector or EGFP-tagged LacZ subcloned into pShooter vector. All of the constructs used here were confirmed by DNA sequence analysis.

* This work was supported by grants from the Ministry of Health, Labor and Welfare of Japan and a Center of Excellence grant from the Ministry of Education, Culture, Sports, Science and Technology of Japan. The costs of publication of this article were defrayed in part by the payment of page charges. This article must therefore be hereby marked "*advertisement*" in accordance with 18 U.S.C. Section 1734 solely to indicate this fact.

‡ To whom correspondence should be addressed. Tel.: 81-52-744-2385; Fax: 81-52-744-2384; E-mail: sobueg@med.nagoya-u.ac.jp.

[1] The abbreviations used are: ALS, amyotrophic lateral sclerosis; FALS, familial amyotrophic lateral sclerosis; SOD1, superoxide dismutase 1; ER, endoplasmic reticulum; EGFP, enhanced green fluorescent protein; PI, propidium iodide; TUNEL, terminal deoxynucleotidyltransferase-mediated UTP end labeling; MTS, 3-(4,5-dimethyl-thiazol-2yl)-5-(3-carboxymethoxyphenyl)-2-(4-sulfophenyl)-2H-tetrazolium; PCD, programmed cell death; COX, cytochrome *c* oxidase; AIF, apoptosis-inducing factor; Smac, second mitochondria-derived activator of caspase; ANOVA, analysis of variance.

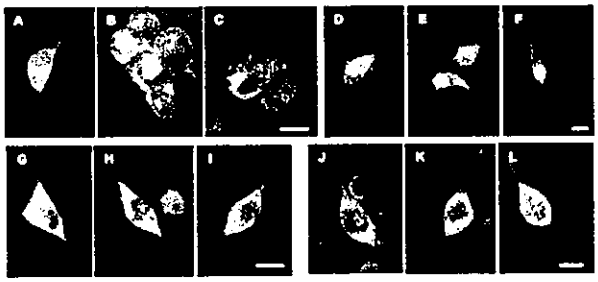

FIG. 1. **Subcellular localization of SOD1-EGFP in Neuro2a cells.** Overlays of two images were taken by laser confocal microscopy 48 h after transfection. *A*, Cyto-wtSOD1; *B*, Cyto-mSOD1^{G93A}; *C*, Cyto-mSOD1^{G85R}; *D*, Nuc-wtSOD1; *E*, Nuc-mSOD1^{G93A}; *F*, Nuc-mSOD1^{G85R}; *G*, ER-wtSOD1; *H*, ER-mSOD1^{G93A}; *I*, ER-mSOD1^{G85R}; *J*, Mito-wtSOD1; *K*, Mito-mSOD1^{G93A}; *L*, Mito-mSOD1^{G85R}. SOD1-EGFP fusion proteins (*green*) were observed comparatively ubiquitous in the cells with Cyto-SOD1 containing no organelle-oriented signals (*A–C*). Only cells with Cyto-mSOD1 contained aggregates of SOD1-EGFP (*B* and *C*). In contrast, each transient expression of organelle-oriented SOD1 (Nuc-, ER-, and Mito-SOD1) was mainly observed in each organelle without aggregate formation regardless wild type or mutant (*D–L*). In cells with Nuc-SOD1, SOD1-EGFP fusion proteins were observed mainly in the nucleus (*D–F*). In the cells with ER-SOD1, SOD1-EGFP fusion proteins were observed mainly in the ER (*G–I*). In the cells with Mito-SOD1, SOD1-EGFP fusion proteins were observed mainly in the mitochondria (*J–L*). The cells were counterstained with propidium iodide (*red*). *Scale bars*, 10 μm.

Cell Culture—Mouse neuroblastoma cell line Neuro2a cells were maintained in Dulbecco's modified Eagle's medium (Invitrogen) supplemented with 10% fetal calf serum (Invitrogen) as described previously (35). They were cultured in Lab-Tec II 4-well chamber slides (Nalge Nunc International) coated with rat tail collagen (Roche Diagnostics). Transient expression of each vector (0.4 μg of DNA/well) in Neuro2a cells (2×10^4 cells/well) was accomplished with LipofectAMINE Plus reagent (Invitrogen). After a 3-h incubation with transfection reagents, the transfected cells were cultured in differentiation medium (Dulbecco's modified Eagle's medium supplemented with 1% fetal calf serum and 20 μM retinoic acid). For treatment with the broad caspase inhibitor (zVAD-fmk; Promega) and the caspase-9-specific inhibitor (zLEHD-fmk; Calbiochem), either 20 μM zVAD-fmk or 20 μM zLEHD-fmk was added at this time.

Cell Fractionation—At each time point (12, 24, and 48 h) after transfection, the cells were collected and gently homogenized with a Dounce homogenizer in cold buffer (250 mM sucrose, 10 mM Tris-HCl, pH 7.5, 5 mM $MgCl_2$, 2 mM EDTA, and protease inhibitor mixture (Complete Mini EDTA-free; Roche Diagnostics)). The homogenates were centrifuged ($600 \times g$, 10 min), and the pellets were designated as the nuclear fractions. The supernatants were centrifuged ($10,000 \times g$, 10 min), and the resulting pellets were designated as the mitochondrial fractions. The supernatants were centrifuged ($100,000 \times g$, 60 min), and the resulting pellets were designated as the microsomal fractions. The supernatants were centrifuged ($300,000 \times g$, 60 min), and the resulting supernatants were designated as the cytosolic fractions. Each pellet was resuspended in TNES buffer (50 mM Tris-HCl, pH 7.5, 150 mM NaCl, 1% Nonidet P-40, 2 mM EDTA, 0.1% SDS, and protease inhibitor mixture (Complete Mini EDTA-free; Roche Diagnostics)). The insoluble debris was briefly pelleted. To verify the fractionation, each fraction was subjected to Western blotting for Sp1 as a nuclear marker using anti-Sp1 rabbit polyclonal antibody (1:1,000, Santa Cruz), cytochrome *c* oxidase (COX) as a mitochondrial marker using a anti-COX subunit IV mouse monoclonal antibody (1:1,000; Molecular Probes), GRP78 as a microsomal marker using anti-GRP78 goat polyclonal antibody (1:1,000; Santa Cruz), and β-actin as a cytosolic marker using anti-β-actin mouse monoclonal antibody (1:5,000; Sigma).

Western Blot Analysis—The protein concentration was determined with a DC protein assay kit (Bio-Rad), and Western blotting was processed as described previously (35). To verify the subcellular localization of SOD1-EGFP fusion proteins, 20 μg of protein from each fraction was loaded. For analyzing the release of cytochrome *c*, apoptosis-inducing factor (AIF), and second mitochondria-derived activator of caspase (Smac) from the mitochondria into the cytosol and for analyzing the translocation of Bax, Bak, Bid, Bad, and Bim from the cytosol into the mitochondria, 20 μg of protein from the mitochondrial fraction or the cytosolic fraction was loaded, and the cells incubated with 10 nM staurosporin for 24 h served as a positive control.

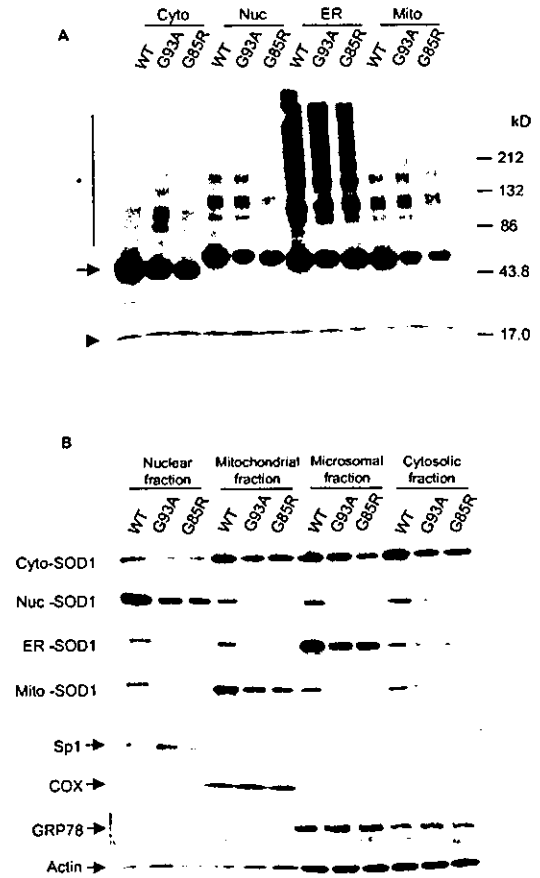

FIG. 2. **Protein level of SOD1-EGFP fusion proteins analyzed by Western blots.** To each well, 20 μg of protein of the sample was applied. *WT*, wtSOD1; *G93A*, mSOD1^{G93A}; *G85R*, mSOD1^{G85R}. *A*, protein levels of SOD1-EGFP fusion proteins 48 h after transfection. The protein level of SOD1-EGFP fusion protein (*arrow*) was much higher than endogenous SOD1 (*arrowhead*). The protein level of the mutant SOD1-EGFP was consistently less than that of wild type SOD1-EGFP regardless of vector type. SOD1 immunoreactive, ladder-like, slowly migrating masses speculated to be SOD1-EGFP oligomers were observed through the gels (*asterisk*), but no significant difference was recognized in the lanes between wtSOD1 and mSOD1. *B*, subcellular localization of SOD1-EGFP fusion proteins 48 h after transfection. Transient expression of SOD1-EGFP fusion protein by Cyto-SOD1 vectors was observed to be comparatively ubiquitous in each cell fraction (*top panel*). In contrast, each transient expression of SOD1-FGFP by organelle-oriented vectors (Nuc-, ER-, and Mito-SOD1) was observed in each organelle (*second*, *third*, and *fourth panels*, respectively.). Sp1, COX, GRP78, and β-actin were used as markers of the nuclear, mitochondrial, microsomal, and cytosolic fraction, respectively.

To assess the protein levels of SOD1-EGFP fusion proteins and the activation of caspase-9 and -3, cells were collected at each time point (12, 24, and 48 h) after transfection and lysed in TNES buffer. Insoluble debris was pelleted, and 20 μg of protein was loaded.

The primary antibodies used here were as follows: anti-SOD1 rabbit polyclonal antibody (1:10,000; StressGen Biotechnologies), anti-caspase-3 rabbit polyclonal antibody, anti-caspase-9 rabbit polyclonal antibody (1:1,000; Cell Signaling), anti-cytochrome *c* mouse monoclonal antibody (1:1,000; BD PharMingen), anti-AIF rabbit polyclonal antibody, anti-Smac goat polyclonal antibody (1:500; Santa Cruz Biotechnology), anti-Bax rabbit polyclonal antibody, anti-Bak rabbit polyclonal antibody, anti-Bad rabbit polyclonal antibody, anti-Bid rabbit polyclonal antibody, and anti-Bim goat polyclonal antibody (1:200; Santa Cruz Biotechnology). After overnight incubation with primary antibodies at 4 °C, each blot was probed with horseradish peroxidase-conjugated anti-rabbit IgG, anti-mouse IgG (1:5,000; Amersham Biosciences) or anti-goat IgG (1:5,000; Santa Cruz Biotechnology). Then they were

visualized with ECL Plus Western blotting detection reagents (Amersham Biosciences). The signal intensity was quantified by densitometry using NIH Image 1.59 software.

Quantitative Assessment of Cytoplasmic Aggregates, Mitochondrial Impairment, and Cell Death—At each time point (12, 24, and 48 h) after transfection, the cells were fixed with 4% paraformaldehyde for 15 min on ice and then permeabilized with 0.05% Triton X-100 at room temperature for 10 min. Next, they were counterstained with 2 μg/ml propidium iodide (PI; Molecular Probes) at room temperature for 10 min and mounted in Gelvatol. A laser confocal scan microscope (MRC1024, Bio-Rad) was used for the morphological analysis, quantitative assessment of aggregates and mitochondrial membrane potentials, and terminal deoxynucleotidyltransferase-mediated UTP end labeling (TUNEL) assay.

For quantitative assessment of aggregates, more than 200 transfected cells in duplicate slides were assessed blindly in three independent trials. The ratio of aggregate-positive cells was calculated as a percentage of such cells among EGFP-positive cells as described previously (25, 35).

For assessment of mitochondrial membrane potential, we used 5,5′,6,6′-tetrachloro-1,1′,3,3′-tetraethylbenzimidazolocarbocyanine iodide (JC-1; Molecular Probes) according to the manufacturer's protocol at each time point (12, 24, and 48 h) after transfection. More than 200 transfected cells in duplicate slides were assessed blindly in three independent trials.

For TUNEL assay, we used the *in situ* cell death detection kit, TMR red (Roche Diagnostics). At each time point (12, 24, and 48 h) after transfection, the TUNEL assay was carried out according to the manufacturer's protocol. As a positive control, we used the EGFP-LacZ transfected cells that were incubated with 10 nM staurosporin for 24 h. More than 200 transfected cells in duplicate slides were assessed blindly in three independent trials.

Cell death was assessed by the dye exclusion method with PI as described previously (25, 35). At each time point (12, 24, and 48 h) after transfection, the cells were incubated with 2 μg/ml PI in Dulbecco's modified Eagle's medium for 15 min at 37 °C and mounted in Gelvatol. More than 200 transfected cells in duplicate slides were assessed blindly in three independent trials under a conventional fluorescent microscope. The ratio of dead cells was calculated as a percentage of PI-positive cells among EGFP-positive cells.

For assessment of cell viability through mitochondrial impairment, we used the 3-(4,5-dimethyl-thiazol-2yl)-5-(3-carboxymethoxyphenyl)-2-(4-sulfophenyl)-2H-tetrazolium (MTS) assay with CellTiter 96 Aqueous one solution assay (Promega). At each time point (12, 24, and 48 h) after transfection, MTS assays were carried out in six independent trials. Absorbance at 490 nm was measured in a multiple plate reader as described previously (13, 25).

Statistical Analysis—All of the results were analyzed by two-way analysis of variance (ANOVA) with Tukey-Kramer post-hoc test using Statview software version 5 (SAS Institute Inc.).

RESULTS

Mito-mSOD1 Induces Significant Cell Death with Lack of Aggregate Formation—Laser confocal microscopic images and Western blots demonstrated that the subcellular localization of SOD1-EGFP fusion proteins expressed by Cyto-SOD1 was comparatively ubiquitous among the subcellular fractions (Figs. 1, *A–C*, and 2*B*). In contrast, each transient expression of organelle-oriented SOD1 (Nuc-, ER-, and Mito-SOD1) was mainly observed in each organelle (Figs. 1, *D–L*, and 2*B*). The protein level of SOD1-EGFP fusion proteins was much higher than endogenous SOD1 (Fig. 2*A*). The protein level of the mutant SOD1-EGFP was consistently less than that of wild type SOD1-EGFP (Fig. 2*A*). As reported previously (32, 35, 36), SOD1 immunoreactive, ladder-like, slowly migrating masses speculated as SOD1-EGFP oligomers were observed through the gels (Fig. 2*A*, *asterisk*), but no constant relation was presented between wtSOD1 and mSOD1 of all vectors. These ladder-like masses were most clearly observed in the lanes of ER-SOD1s, especially ER-wtSOD1 (Fig. 2*A*).

As we previously demonstrated (35), the cells with Cyto-mSOD1 developed cell death and cytoplasmic aggregates of SOD1-EGFP fusion proteins, whereas those with Cyto-wtSOD1 did not (Figs. 1, *A–C*, and 3). The cells with Mito-mSOD1

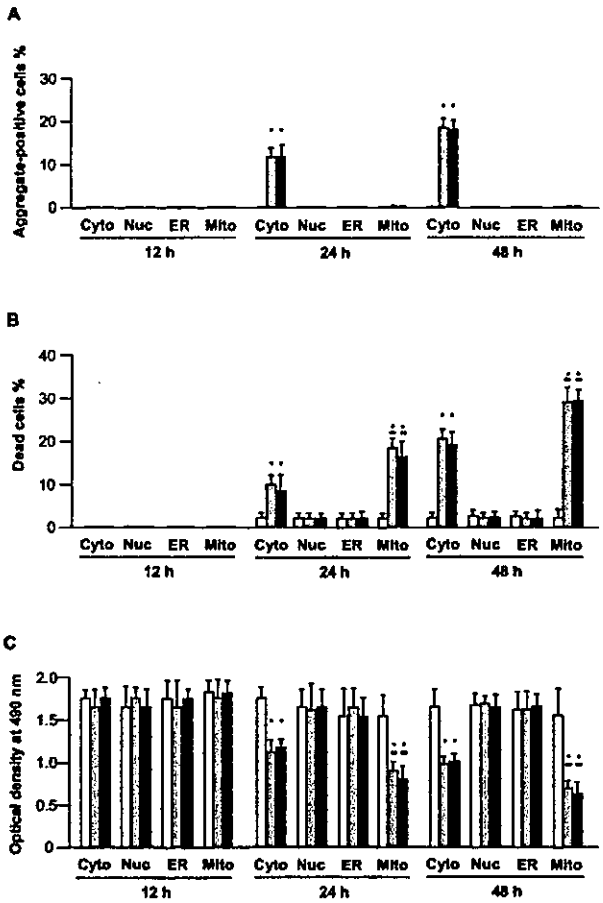

FIG. 3. **Frequency of aggregate-positive cells and dead cells and MTS assay.** *A*, frequency of aggregate-positive cells. *B*, frequency of dead cells. *C*, MTS assay. *White columns*, wtSOD1; *gray columns*, mSOD1^{G93A}; *black columns*, mSOD1^{G85R}; *Cyto*, Cyto-SOD1; *Nuc*, Nuc-SOD1; *ER*, ER-SOD1; *Mito*, Mito-SOD1. *, $p < 0.001$ *versus* wtSOD1 of each vector; **, $p < 0.05$ *versus* Cyto-mSOD1 (by two-way ANOVA with Tukey-Kramer post-hoc test). The values are the means ± S.D. ($n = 6$).

exhibited a more significant level of cell death and mitochondrial impairment than those with Cyto-mSOD1 but did not develop cytoplasmic aggregates (Figs. 1, *K* and *L*, and 3). The cells with Nuc-wt and mSOD1, ER-wt and mSOD1, or Mito-wtSOD1 did not develop cytoplasmic aggregates or show cell death (Figs. 1, *D–J*, and 3). Expression of either the empty vector or the control vector alone did not induce cytoplasmic aggregates and cell death (data not shown). These findings suggest that the localization of mSOD1 in the mitochondria plays a critical role in mSOD1-mediated cytotoxicity, whereas cytoplasmic aggregate formation or oligomeric formation does not. Furthermore, Cyto-mSOD1-induced cell death, which was less significant than Mito-mSOD1-induced cell death, could be mediated by mitochondrial localization of mSOD1 because a moderate amount of mSOD1 was present in the mitochondria.

Mito-mSOD1 Induces Mitochondrial Cytochrome c Release Followed by Sequential Activation of Caspase-9 and -3—We assessed which mitochondrial death signal was involved in mSOD1-mediated cytotoxicity. Western blots revealed that cytochrome *c* release from the mitochondria into the cytosol occurred in the cells with Mito-mSOD1 (Fig. 4*A*). The cells with Cyto-mSOD1 also elicited less cytochrome *c* release (Fig. 4*A*), whereas it did not occur in the cells with Nuc-mSOD1 or ER-mSOD1 (data not shown). The time course of densitometric analysis revealed that the cytochrome *c* release in the cells

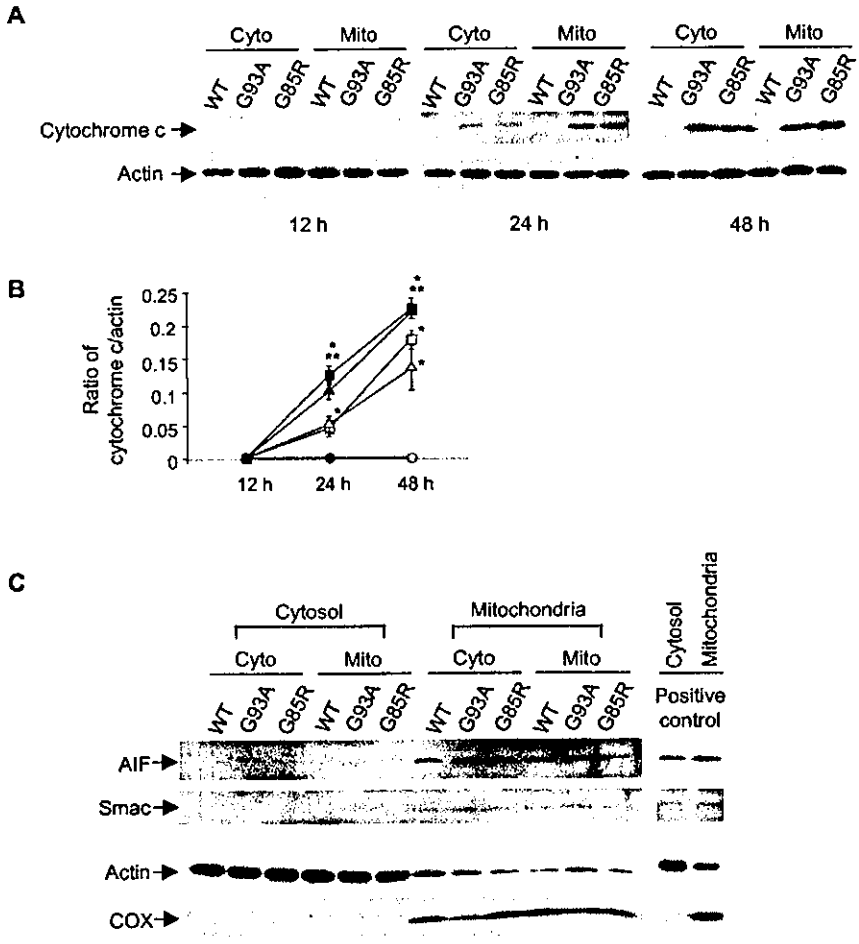

FIG. 4. **Western blot analysis of cytochrome *c*, AIF, and Smac.** *A*, time course of the mitochondrial cytochrome *c* release into the cytosol. *B*, densitometric analysis of cytochrome *c* release. *C*, subcellular localization of AIF and Smac 48 h after transfection. COX and β-actin were used as markers of the mitochondrial and cytosolic fraction, respectively. *WT*, wt-SOD1; *G93A*, mSOD1^{G93A}; *G85R*, mSOD1^{G85R}; *Cyto*, Cyto-SOD1; *Mito*, Mito-SOD1. ○, Cyto-wtSOD1; △, Cyto-mSOD1^{G93A}; □, Cyto-mSOD1^{G85R}; ●, Mito-wtSOD1; ▲, Mito-mSOD1^{G93A}; ■, Mito-mSOD1^{G85R}. *, $p < 0.001$ *versus* wt-SOD1 of each vector; **, $p < 0.05$ *versus* Cyto-mSOD1 (by two-way ANOVA with Tukey-Kramer post-hoc test). The values are the means ± S.D. ($n = 3$).

with Mito-mSOD1 increased gradually and was significantly stronger than those with Cyto-mSOD1 (Fig. 4*B*). Because AIF and Smac are also known as the signal proteins released from the mitochondria into the cytosol that promote apoptosis (37, 38), we examined the release of these mitochondrial proteins into the cytosol in this model. Western blots were not able to detect the release of AIF and Smac in the cells with either Cyto-mSOD1 or Mito-mSOD1 (Fig. 4*C*). Thus, AIF and Smac did not seem to be involved in the neuronal cell death in our model.

Then we examined the downstream signal cascade of the activation of caspase-9 and -3 following the mitochondrial cytochrome *c* release. Western blots demonstrated that the caspase-9 and -3 were activated in the cells with Cyto-mSOD1 and those with Mito-mSOD1, whereas they were not activated in the cells with Cyto-wtSOD1 and those with Mito-wtSOD1 (Fig. 5*A*, *lanes 1–18*). The time course of densitometric analysis revealed that caspase-9 and -3 were activated gradually and sequentially, and both activations were significantly stronger in the cells with Mito-mSOD1 than those with Cyto-mSOD1 (Fig. 5, *B* and *C*).

Bcl-2 Family Pro-apoptotic Proteins Are Not Involved in Cyto-mSOD1 and Mito-mSOD1-induced Cell Death—Bcl-2 family pro-apoptotic proteins such as Bax, Bak, Bid, Bad, and Bim were considered to be translocated from the cytosol to the mitochondria during apoptosis and to promote the mitochondrial cytochrome *c* release to the cytosol (37–39). Thus, we examined whether Bax, Bak, Bid, Bad, and Bim were involved in the cytochrome *c* release in this model. Western blots, however, did not show the translocation of these proteins to the mitochondria (Fig. 5*D*). We also assessed the alteration of mitochondrial membrane potential with JC-1 but were unable to detect a significant difference in the ratio of JC-1 monomer and J aggregates between the cells with wtSOD1 and those with mSOD1 of any vectors (data not shown). These data suggested that mitochondrial localization of mutant SOD1 elicited cytochrome *c* release from the mitochondria to the cytosol followed by caspase activation without involvement of Bcl-2 family pro-apoptotic protein translocation and mitochondrial membrane potential alterations.

Caspase-9-specific Inhibitor and Broad Caspase Inhibitor Prevented Mitochondrial-localized Mutant SOD1-mediated Cell Death—To determine whether the mitochondrial-dependent caspase cascade activation plays a role in the mSOD1-mediated cell death, we examined the effect of treatments with the broad caspase inhibitor (zVAD-fmk) and the caspase-9-specific inhibitor (zLEHD-fmk). Western blots indicated that treatment with 20 μM zVAD-fmk or 20 μM zLEHD-fmk completely blocked the activation of caspase-9 and -3 (Fig. 5*A*, *lanes 19–30*) and diminished mSOD1-mediated cell death and mitochondrial impairment (Fig. 6) in the cells with Mito-mSOD1 as well as Cyto-mSOD1. No significant difference was observed in the inhibitory effect of zVAD-fmk and zLEHD-fmk (Fig. 6). These findings suggest that the pathway from release of cytochrome *c* to activation of caspase-9 and caspase-3 is the main process of mSOD1-mediated neuronal cell death.

Despite the activation of caspase-3, the cells with Cyto-mSOD1 or Mito-mSOD1 showed TUNEL-negative staining as

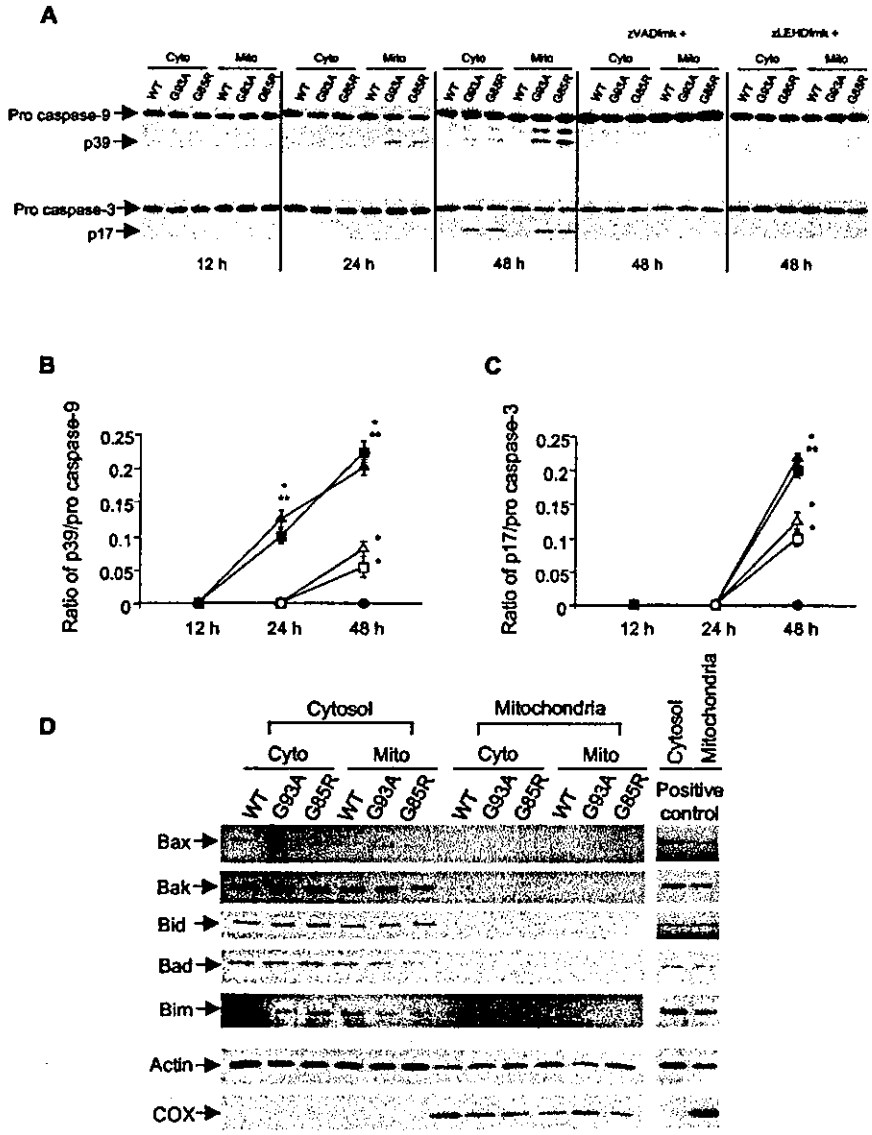

FIG. 5. **Western blot analysis of caspase-9 and -3 and Bcl-2 family pro-apoptotic proteins.** *A*, time course of the activation of caspase-9 and -3. *B*, densitometric analysis of caspase-9 activation. *C*, densitometric analysis of caspase-3 activation. *D*, subcellular localization of Bcl-2 family pro-apoptotic proteins 48 h after transfection. COX and β-actin were used as markers of the mitochondrial and cytosolic fraction, respectively. *WT*, wtSOD1; *G93A*, mSOD1^{G93A}; *G85R*, mSOD1^{G85R}; *Cyto*, Cyto-SOD1; *Mito*, Mito-SOD1. ○, Cyto-wtSOD1; △, Cyto-mSOD1^{G93A}; □, Cyto-mSOD1^{G85R}; ●, Mito-wtSOD1; ▲, Mito-mSOD1^{G93A}; ■, Mito-mSOD1^{G85R}. *, $p < 0.001$ *versus* wt-SOD1 of each vector; **, $p < 0.05$; *versus* Cyto-mSOD1 (by two-way ANOVA with Tukey-Kramer post-hoc test). The values are the means ± S.D. ($n = 3$).

well as those with Cyto-wtSOD1 or Mito-wtSOD1 (Fig. 7, *A–F*), whereas cells treated with staurosporin exhibited obvious TUNEL-positive staining and nuclear pycnosis (Fig. 7, *G–I*).

DISCUSSION

Here we provided unequivocal evidence that mitochondrial localization of mutant SOD1 is the essential part of mutant SOD1-mediated neurotoxicity in a cellular model of FALS. First, neuronal cell death was elicited when mutant SOD1 was localized in the mitochondria, not in the nucleus nor ER, and was not associated with cytoplasmic aggregate formation. Second, the extent of cytochrome *c* release and following caspase-9 and -3 activation were markedly enhanced by accumulation of mutant SOD1 in the mitochondria. Third, Bcl-2 family pro-apoptotic proteins such as Bax, Bak, Bid, Bad, and Bim and the mitochondrial membrane potential alterations were not involved in the cytochrome *c* release from the mitochondria into the cytosol in our model. Fourth, a caspase-9-specific inhibitor zLEHD-fmk as well as a broad caspase inhibitor zVAD-fmk diminished mutant SOD1-mediated neuronal cell death. Thus, the localization of mutant SOD1 in the mitochondria triggers the cytochrome *c* release followed by caspase-dependent neuronal cell death independent of Bcl-2 family pro-apoptotic proteins and alteration of mitochondrial membrane potentials. Furthermore, mutant SOD1-mediated cell death was independent of cytoplasmic aggregate formation. A previous study reported that Bax translocation from the cytosol to the mitochondria was associated with cytochrome *c* release from the mitochondria into the cytosol in the FALS transgenic mice model (20), but there is a possibility that the surroundings of motor neurons such as astorocytes or dying neurons might affect Bax translocation in the model used.

Mitochondrial involvement in ALS and FALS has been documented (18–26). Mitochondrial degeneration of vacuolation or membrane disintegration in motor neurons is one of the earliest pathological findings in FALS transgenic mice (2, 5, 8, 9). Moreover, mitochondrial dysfunctions such as altered calcium homeostasis (18), decrease in respiratory chain complex activity (22, 23), alteration of the mitochondria-related gene expression (24), and increase in reactive oxygen species (39) have been reported in *in vitro* and *in vivo* models. Recent studies revealed that SOD1, which has been considered to be a cytosolic enzyme, also exists in the mitochondria (25–27) and that

mutant SOD1 was present in the vacuolated mitochondria of FALS transgenic mice model (27). Previous studies also revealed that cytochrome *c* release and subsequent caspase activation occurred (20, 21, 25, 40–43) and that inhibition of cytochrome *c* release by minocycline (21), coexpression of X chromosome-linked inhibitor of apoptosis protein (25), and treatment with a broad caspase inhibitor zVAD-fmk (42) inhibited cell death in the *in vitro* and *in vivo* models of FALS. In this study, we unequivocally demonstrated that mitochondrial localization of mutant SOD1 itself is primary and crucial to elicit the following mitochondrial death signals for mutant SOD1-mediated neuronal cell death. The cells with Cyto-mSOD1 showed a lesser extent of cell death than those with Mito-SOD1, probably because mutant SOD1 by Cyto-mSOD1 accumulated less in the mitochondria than that by Mito-SOD1.

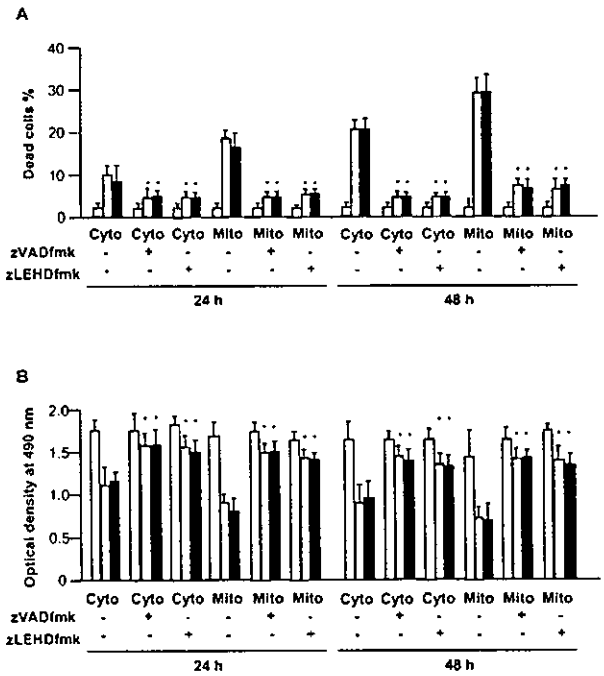

FIG. 6. **Frequency of dead cells and MTS assay after treatment with caspase inhibitors.** *A*, frequency of dead cells. *B*, MTS assay. *White columns*, wtSOD1; *gray columns*, mSOD1^{G93A}; *black columns*, mSOD1^{G85R}; *Cyto*, Cyto-SOD1; *Mito*, Mito-SOD1. *, $p < 0.001$ *versus* untreated mSOD1 of each vector (by two-way ANOVA with Tukey-Kramer post-hoc test). The values are the means ± S.D. ($n = 6$).

In the present study, similar to previous reports (32, 35, 36), SOD1 immunoreactive, ladder-like, slowly migrating masses speculated to be SOD1-EGFP oligomers were observed on Western blots (Fig. 2*A*, *asterisk*), but no significant difference was detected between wtSOD1 and mSOD1 of all vectors. These ladder-like masses were most clearly observed in the ER-SOD1s, probably because SOD1-EGFP fusion proteins with ER retention signals may avoid proteasome-mediated degradation and tend to accumulate in the ER as an unfolded form. The level of these ladder-like, slowly migrating masses was not associated with neuronal cell death, but there remains the possibility that localization of mutant SOD1 oligomers in the mitochondria may cause neurotoxicity. The mitochondrial quality control system depends on ATP-dependent protease complexes such as homologues of Lon and Hsp70 (44–46). However, the capacity of mitochondria to deal with abnormal proteins might be rather limited, and the mitochondria seem to release death signals when abnormal proteins overflowed. Further investigations are needed to give an answer to this issue.

Cytoplasmic aggregate formation containing mutant SOD1 is a hallmark of mutant SOD1-associated FALS, and it has been demonstrated in the *in vitro* and *in vivo* FALS models (2, 4–9). These aggregates have been considered to participate in

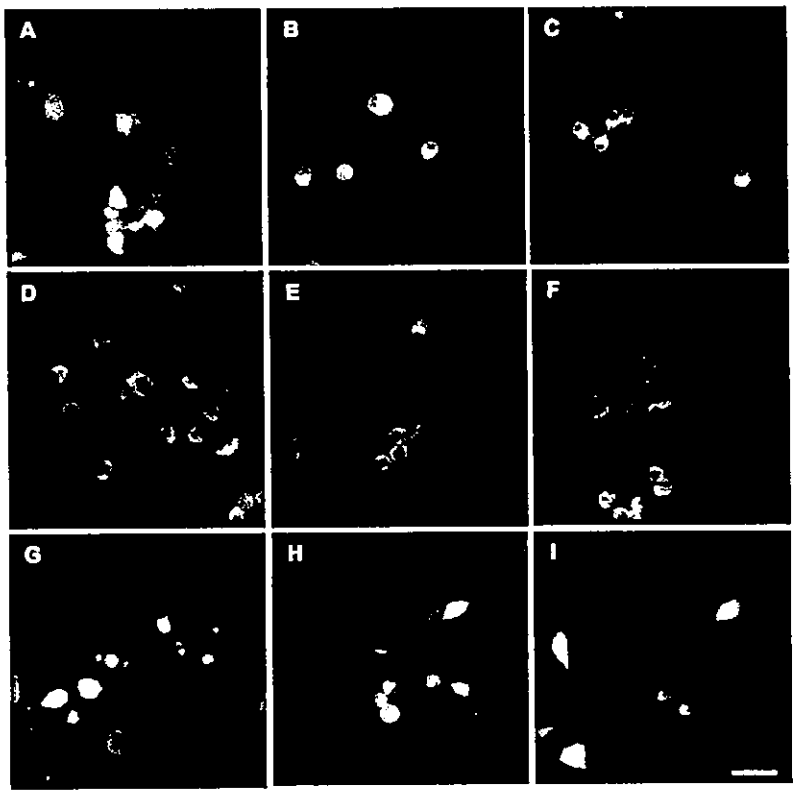

FIG. 7. **TUNEL assay.** Overlays of two images were taken by laser confocal microscopy 48 h after transfection. *A*, Cyto-wtSOD1; *B*, Cyto-mSOD1^{G93A}; *C*, Cyto-mSOD1^{G85R}; *D*, Mito-wtSOD1; *E*, Mito-mSOD1^{G93A}; *F*, Mito-mSOD1^{G85R}; *G–I*, EGFP-LacZ transfected cells incubated with 0.01 μM staurosporin for 24 h as positive controls (red nuclear staining in pycnotic cells). The cells with Cyto-mSOD1 (*B* and *C*) or Mito-SOD1 (*E* and *F*) showed negative staining as well as those with wtSOD1 (*A* and *D*). *Scale bar*, 30 μm.

a pathogenic process (30), although this has been disputed (31–33, 35). In this study, we conclusively demonstrated that cytoplasmic aggregates are not directly associated with cell death, similar to the *in vivo* models of polyglutamine diseases, suggesting that the subcellular localization of mutant protein itself, rather than aggregate formation, exerts toxicity (14, 30).

Controversy surrounds the issue of whether the motor neuronal cell death in mutant SOD1-associated FALS is apoptosis (47, 48) or not (49). A previous study on an *in vivo* model reported that activated caspase-3-positive motor neurons were observed, but TUNEL-positive motor neurons were not (43). Similarly, we were unable to find TUNEL-positive cells despite obvious activation of caspase-3. Recently, at least three types of programmed cell death (PCD) have been proposed: apoptosis, apoptosis-like PCD, and necrosis-like PCD (50). Apoptosis-like PCD is cell death with less chromatin condensation than in apoptosis or any degree and combination of apoptotic features such as caspase activation, cytoplasmic shrinkage, and plasma membrane blebbing (50). Previous reports suggested that apoptosis-like PCD may be a type of neuronal cell death in neurodegenerative diseases including ALS (51, 52). The present study also indicated the possibility that this apoptosis-like PCD is a type of neuronal cell death through the mitochondrial signal pathway in motor neurons with mutant SOD1. However, further investigations are needed to shed light on the mechanism of mutant SOD1-mediated neuronal cell death.

In conclusion, in this study we demonstrated that mitochondrial localization of mutant SOD1 itself triggers cytochrome *c* release from the mitochondria into the cytosol that initiates the caspase-dependent cell death cascade in a FALS model. Inhibition of mitochondrial localization of mutant SOD1 may well be a candidate for a therapeutic approach to FALS.

Acknowledgments—We are grateful to Dr. Keiji Tanaka (Department of Molecular Oncology, The Tokyo Metropolitan Institute of Medical Science) and Dr. Jun-ichi Niwa (Department of Neurology, Nagoya University Graduate School of Medicine) for helpful discussion. We also thank Dr. Kumi Kawai (Department of Pathology, Nagoya University Graduate School of Medicine) for technical assistance.

REFERENCES

1. Rosen, D. R., Siddique, T., Patterson, D., Figlewicz, D. A., Sapp, P., Hentati, A., Donaldson, D., Goto, J., O'Regan, J. P., Deng, H. X., Rahmani, Z., Krizus, A., McKenna-Yasek, D., Cayabyab, A., Gaston, S. M., Berger, R., Tanzi, R. E., Halperin, J. J., Herzfeldt, B., den Bergh, R. V., Hung, W. Y., Bird, T., Deng, G., Mulder, D. W., Smyth, C., Laing, N. G., Soriano, E., Pericak-Vance, M. A., Haines, J., Rouleau, G. A., Gusella, J. S., Horvitz, H. R., and Brown, R. H. (1993) *Nature* **362**, 59–62
2. Hirano, A. (1996) *Neurology* **47**, (Suppl. 2) S63–S66
3. Yim, M. B., Kang, J. H., Yim, H. S., Kwak, H. S., Chock, P. B., and Stadtman, E. R. (1996) *Proc. Natl. Acad. Sci. U. S. A.* **93**, 5709–5714
4. Wong, P. C., Pardo, C. A., Borchelt, D. R., Lee, M. K., Copeland, N. G., Jenkins, N. A., Sisodia, S. S., Cleveland, D. W., and Price, D. L. (1995) *Neuron* **14**, 1105–1116
5. Dal Canto, M. C., and Gurney, M. E. (1994) *Am. J. Pathol.* **145**, 1271–1279
6. Shibata, N., Hirano, A., Kobayashi, M., Siddique, T., Deng, H. X., Hung, W. Y., Kato, T., and Asayama, K. (1996) *J. Neuropathol. Exp. Neurol.* **55**, 481–490
7. Shibata, N., Hirano, A., Kobayashi, M., Dal Canto, M. C., Gurney, M. E., Komori, T., Umahara, T., and Asayama, K. (1998) *Acta Neuropathol.* **95**, 136–142
8. Kong, J., and Xu, Z. (1998) *J. Neurosci.* **18**, 3241–3250
9. Jaarsma, D., Haasdijk, E. D., Grashorn, J. A. C., Hawkins, R., van Duijn, W., Verspaget, H. W., London, J., and Holstege, J. C. (2000) *Neurobiol. Dis.* **7**, 623–643
10. Klement, I. A., Skinner, P. J., Kaytor, M. D., Yi, H., Hersch, S. M., Clark, H. B., Zoghbi, H. Y., and Orr, H. T. (1998) *Cell* **95**, 41–53
11. Saudou, F., Finkbeiner, S., Devys, D., and Greenberg, M. E. (1998) *Cell* **95**, 55–66
12. Schilling, G., Wood, J. D., Duan, K., Slunt, H. H., Gonzales, V., Yamada, M., Cooper, J. K., Margolis, R. L., Jenkins, N. A., Copeland, N. G., Takahashi, H., Tsuji, S., Price, D. L., Borchelt, D. R., and Ross, C. A. (1999) *Neuron* **24**, 275–286
13. Kobayashi, Y., Kume, A., Li, M., Doyu, M., Hata, M., Ohtsuka, K., and Sobue, G. (2000) *J. Biol. Chem.* **275**, 8772–8778
14. Katsuno, M., Adachi, H., Kume, A., Li, M., Nakagomi, Y., Niwa, H., Sang C., Kobayashi, Y., Doyu, M., and Sobue, G. (2002) *Neuron* **35**, 843–854
15. Mattson, M. P., Guo, Q., Furukawa, K., and Pedersen, W. A. (1998) *J. Neurochem.* **70**, 1–14
16. Katayama, T., Imaizumi, K., Honda, A., Yoneda, T., Kudo, T., Takeda, M., Mori, K., Rozmahel, R., Fraser, P., George-Hyslop, P. S., and Tohyama, M. (2001) *J. Biol. Chem.* **276**, 43446–43454
17. Imai, Y., Soda, M., Inoue, H., Hattori, N., Mizuno, Y., and Takahashi, R. (2001) *Cell* **105**, 891–902
18. Carrì, M. T., Ferri, A., Battistoni, A., Famhy, L., Gabbianelli, R., Poccia, F., and Rotilio, G. (1997) *FEBS Lett.* **414**, 365–368
19. Beal, M. F. (2000) *Brain* **123**, 1291–1292
20. Guégan, C., Vila, M., Rosoklija, G., Hays, A. P., and Przedborski, S. (2001) *J. Neurosci.* **21**, 6569–6576
21. Zhu, S., Stavrovskaya, I. G., Drozda, M., Kim, B. Y., Ona, V., Li, M., Sarang, S., Liu, A. S., Hartley, D. M., Wu, D. C., Gullans, S., Ferrante, R. J., Przedborski, S., Kristal, B. S., and Friedlander, R. M. (2002) *Nature* **417**, 74–78
22. Menzies, F. M., Cookson, M. R., Taylor, R. W., Turnbull, D. M., Chrzanowska-Lightowlers, Z. M., Dong, L., Figlewicz, D. A., and Shaw, P. J. (2002) *Brain* **125**, 1522–1533
23. Mattiazzi, M., D'Aurelio, M., Gajewski, C. D., Martushova, K., Kiaei, M., Beal, M. F., and Manfredi, G. (2002) *J. Biol. Chem.* **277**, 29626–29633
24. Yoshihara, T., Ishigaki, S., Yamamoto, M., Liang, Y., Niwa, J., Takeuchi, H., Doyu, M., and Sobue, G. (2002) *J. Neurochem.* **80**, 158–167
25. Ishigaki, S., Liang, Y., Yamamoto, M., Niwa, J., Ando, Y., Yoshihara, T., Takeuchi, H., Doyu, M., and Sobue, G. (2002) *J. Neurochem.* **82**, 576–584
26. Menzius, F. M., Ince, P. G., and Shaw, P. J. (2002) *Neurochem. Int.* **40**, 543–551
27. Sturtz, L. A., Diekert, K., Jensen, L. T., Lill, R., and Culotta, V. C. (2001) *J. Biol. Chem.* **276**, 38084–38089
28. Jaarsma, D., Rognoni, F., van Duijn, W., Verspaget, H. W., Haasdijk, E. D., and Holstege, J. C. (2001) *Acta Neuropathol.* **102**, 293–305
29. Higgins, C. M., Jung, C., Ding, H., and Xu, Z. (2002) *J. Neurosci.* **22**, RC215
30. Bruijin, L. I., Houseweart, M. K., Kato, S., Anderson, K. L., Anderson, S. D., Ohama, E., Reaume, A. G., Scott, R. W., and Cleveland, D. W. (1998) *Science* **281**, 1851–1854
31. Cummings, C. J., Reinstein, E., Sun, Y., Antalffy, B., Jiang, Y., Ciechanover, A., Orr, H. T., Beaudet, A. L., and Zoghbi, H. Y. (1999) *Neuron* **24**, 879–892
32. Johnston, J. A., Dalton, M. J., Gurney, M. E., and Kopito, R. R. (2000) *Proc. Natl. Acad. Sci. U. S. A.* **97**, 12571–12576
33. Kopito, R. R. (2000) *Trends Cell Biol.* **10**, 524–530
34. Bruening, W., Roy, J., Giasson, B., Figlewicz, D. A., Mushynski, W. E., and Durham, H. D. (1999) *J. Neurochem.* **72**, 693–699
35. Takeuchi, H., Kobayashi, Y., Yoshihara, T., Niwa, J., Doyu, M., Ohtsuka, K., and Sobue, G. (2002) *Brain Res.* **949**, 11–22
36. Wang, J., Xu, G., and Borchelt, D. R. (2002) *Neurobiol. Dis.* **9**, 139–148
37. Matsuyama, S., and Reed, J. C. (2000) *Cell Death. Differ.* **7**, 1155–1165
38. Gupta, S. (2001) *Life Sci.* **69**, 2957–2964
39. Green, D. R., and Reed, J. C. (1998) *Science* **281**, 1309–1312
40. Adams, J. M., and Cory, S, (1998) *Science* **281**, 1322–1326
41. Lee, M. H., Hyun, D.-H., Halliwell, B., and Jenner, P. (2001) *J. Neurochem.* **78**, 209–220
42. Li, M., Ona, V. O., Guégan, C., Chen, M., Jackson-Lewis, V., Andrews, L. J., Olszewski, A. J., Stieg, P. E., Lee, J.-P., Przedborski, S., and Friedlander, R. M. (2000) *Science* **288**, 335–339
43. Pasinelli, P., Houseweart, M. K., Brown, R. H., Jr., and Cleveland, D. W. (2000) *Proc. Natl. Acad. Sci. U. S. A.* **97**, 13901–13906
44. Wang, N., Gottesman, S., Willingham, M. C., Gottesman, M. M., and Maurizi, M. R. (1993) *Proc. Natl. Acad. Sci. U. S. A.* **90**, 11247–11251
45. Wang, N., Maurizi, M. R., Emmert-Buck, L., and Gottesman, M. M. (1994) *J. Biol. Chem.* **269**, 29308–29313
46. Okado-Matsumoto, A., and Fridovich, I. (2002) *Proc. Natl. Acad. Sci. U. S. A.* **99**, 9010–9014
47. Durham, H. D., Roy, J., Dong, L., and Figlewicz, D. A. (1997) *J. Neuropathol. Exp. Neurol.* **56**, 523–530
48. Martin, L. J. (1999) *J. Neuropathol. Exp. Neurol.* **58**, 459–471
49. Bendotti, C., Calvaresi, N., Chiveri, L., Prelle, A., Moggio, M., Braga, M., Silani, V., and De Biasi, S. (2001) *J. Neurol. Sci.* **191**, 25–33
50. Leist, M., and Jäättelä, M. (2001) *Nat. Rev. Mol. Cell. Biol.* **2**, 589–598
51. Turmaine, M., Raza, A., Mahal, A., Mangiarini, L., Bates, G. P., and Davies, S. W. (2000) *Proc. Natl. Acad. Sci. U. S. A.* **97**, 8093–8097
52. Sperandio, S., de Belle, I., and Bredesen, D. E. (2000) *Proc. Natl. Acad. Sci. U. S. A.* **97**, 14376–14381

FEBS Letters 531 (2002) 354–358 FEBS 26692

Differentially expressed genes in sporadic amyotrophic lateral sclerosis spinal cords – screening by molecular indexing and subsequent cDNA microarray analysis

Shinsuke Ishigaki[a], Jun-ichi Niwa[a], Yoshio Ando[a], Tsuyoshi Yoshihara[a], Ko-ichi Sawada[a], Manabu Doyu[a], Masahiko Yamamoto[a], Kikuya Kato[b], Yoshihisa Yotsumoto[c], Gen Sobue[a,*]

[a] *Department of Neurology, Nagoya University Graduate School of Medicine, Nagoya 466-0085, Japan*
[b] *Taisho Laboratory of Functional Genomics, Nara Institute of Science and Technology, Nara 630-0101, Japan*
[c] *Pharmaceutical Research Division Discovery Technology Laboratory, Mitsubishi Pharma Corporation, Yokohama 227-0033, Japan*

Received 1 August 2002; revised 27 September 2002; accepted 27 September 2002

First published online 16 October 2002

Edited by Ned Mantei

Abstract To analyze the genes related to the pathophysiology of sporadic amyotrophic lateral sclerosis (SALS) we performed gene profiling of SALS spinal cords using molecular indexing combined with cDNA microarray. Eighty-four fragments were cloned in the first screening procedure with molecular indexing. Subsequent quantitative microarray screening revealed 11 genes which were differentially expressed in SALS. Real-time RT-PCR verified that the expression level of the following six genes was altered in SALS: dorfin, metallothionein-3, 30 kDa TATA-binding protein-associated factor, neugrin, ubiquitin-like protein 5 and macrophage-inhibiting factor-related protein-8. These results indicated that genes associated with the ubiquitin–proteasome system, oxidative toxicity, transcription, neuronal differentiation and inflammation might be involved in the pathogenesis of SALS.

Key words: Amyotrophic lateral sclerosis; Gene expression profile; Molecular indexing; Dorfin; Neugrin

1. Introduction

Amyotrophic lateral sclerosis (ALS) is one of the most common neurodegenerative disorders, characterized by selective motor neuron degeneration in the spinal cord, brainstem and cortex. Approximately 10% of ALS is familial, and 10–20% of these familial ALS (FALS) cases are caused by missense mutations in the Cu/Zn superoxide dismutase (SOD1) gene [1], while others are considered to be sporadic ALS (SALS). Although the etiology of SALS is not known, a great number of studies to date have proposed possible mechanisms of the motor neuron degeneration in SALS. These include oxidative toxicity, glutamate receptor abnormality, ubiquitin–proteasome dysfunction, inflammatory and cytokine activation, dysfunction in neurotrophic factors, damage to mitochondria, cytoskeletal abnormalities and activation of the apoptosis pathway [2,3]. One of the most promising strategies to identify pathophysiologically related molecules in SALS would be the comparison of gene expression profiles of human SALS spinal cords with those of normal controls by the gene expression profiling technique. The spectrum of obtained genes differentially expressed in SALS tissues from normal control tissues would largely depend on the screening systems employed and tissue samples used, particularly in postmortem tissues. Used for human postmortem samples this approach could yield not otherwise obtainable information on the molecular pathophysiology of neuronal degenerations. The only report of large-scale gene profiling on SALS tissues to date, using membrane arrays, has documented that genes involved in oxidative toxicity, neuroinflammation, apoptosis, and lipid metabolism were up-regulated in the spinal cords of SALS patients [4]. We previously used microarray analysis to detect differentially expressed genes in FALS transgenic mice, showing that inflammation- and apoptosis-related genes were up-regulated in G93A-SOD1 transgenic mice [5]. These results indicated that molecules with similar functions were associated with the pathogenesis of both SALS and FALS; however, it is only able to explain the partial pathomechanism for SALS motor neuron degeneration. To identify genes differentially expressed in the SALS spinal cord, particularly novel or low-abundant genes, we adopted molecular indexing, a PCR-based screening procedure, for the primary screening and performed subsequent cDNA microarray analysis.

2. Materials and methods

2.1. Subjects

Postmortem spinal cords samples at segments L3–L5 were taken from eight SALS patients and eight non-neurological disease controls after obtaining their informed consent. Each SALS case was clinically and pathologically verified. Diagnostic criteria for ALS were based on the El Escorial criteria outlined by the World Federation of Neurology [6]. Bunina body inclusions and hyaline ubiquitinated inclusions were detected in the residual motor neurons in all SALS cases. One SALS case (ALS1) and a control (C1) were used for the molecular indexing. Five cases each (ALS1–5 and C1–5) were analyzed for the second screening, microarray analysis. For verification, real-time RT-PCR with TaqMan probe was performed on all cases (Table 1). Each autopsy was performed within 9 h post mortem, and spinal cord samples of lumbar segments (L4/L5) were snap frozen in liquid nitrogen, then stored at −80°C until use. Total RNA was isolated from anterior horn specimens, where motor neurons exist, using the Micro RNA Isolation Kit (Stratagene, La Jolla, CA, USA), and it was reverse transcribed by MMLV reverse transcriptase, Superscript II (Life Technologies, Grand Island, NY, USA).

*Corresponding author. Fax: (81)-52-744-2384.
E-mail address: sobueg@med.nagoya-u.ac.jp (G. Sobue).

0014-5793/02/$22.00
PII: S0014-5793(02)03546-9

2.2. Molecular indexing and collection of screened cDNAs

SALS (ALS1) and control (C1) spinal cords were used for molecular indexing. Briefly, after synthesizing from total RNA, double-stranded cDNA was cut with one of three class IIS restriction enzymes, *Bsm*FI, *Bsm*AI or *Fok*I, and ligated to each of 64 biotinylated adapters cohesive to all possible overhangs. Ligated molecules were digested by the other class IIS restriction enzymes, and were recovered with streptavidin-coated paramagnetic beads. PCR was performed with the adapter primer and an anchored oligo-dT primer. The amplified fragments were separated by polyacrylamide gel electrophoresis. By carrying out the experiment with 64 adapters, three enzymes and three anchored oligo-dT primers, a total of 576 profiles of cDNAs were established. This procedure has been described in detail in previous reports [7,8].

The 576 profiles obtained from the SALS spinal cords were compared with those from the controls, and the cDNA fragments with an apparent difference in peak between the ALS spinal cord and control were chosen as candidate gene fragments. The standard used for this selection was that ratios between SALS and control were more than 5 or less than 0.2. The purified PCR products were inserted into pGEM T-Easy vector (Promega). The insert was sequenced using an autosequencer. The sequence was applied to the search for the information using BLAST of NCBI on the web.

2.3. Screening by custom-spotted cDNA microarray

The cDNA fragments obtained were amplified and spotted on glass arrays in duplicate (DNA Chip Research, Kanagawa, Japan). The samples of total RNA (5 μg) were reverse transcribed into first-strand cDNA using 20 U Superscript II and 1 μl of 0.5 mg/ml T7-oligo-dT primer (5′-TCT AGT CGA CGG CCA GTG AAT TGT AAT ACG ACT CAC TAT AGG GCG T_{21}-3′) at 42°C for 1 h in 20 μl of reaction [1×first-strand reaction buffer, 10 mM dithiothreitol (DTT), 0.25 mM dNTPs, 20 U RNasin (Promega, Madison, WI, USA)]. Next, 30 μl of 5×second-strand synthesis buffer, 3 μl of 10 mM dNTPs, 4 μl DNA polymerase I, 1 μl *Escherichia coli* RNase H, 1 μl *E. coli* DNA ligase and 92 μl of RNase-free H_2O were added, incubated at 16°C for 2 h, then incubated at 16°C for 10 min after the addition of 2 μl of T4 DNA polymerase. The double-stranded cDNA was extracted with 150 μl of phenol–chloroform to eliminate proteins and then purified using a Microcon-100 column (Millipore, Tokyo, Japan) to separate out the unincorporated nucleotides and salts. RNA amplification was performed using Ampliscribe T7 Transcription Kit (Epicentre Technologies, Madison, WI, USA) in a mixture of 8 μl double-stranded cDNA, 2 μl of 10×Ampliscribe T7 buffer, 1.5 μl each of 100 mM ATP, CTP, GTP and UTP, 2 μl 0.1 M DTT and 2 μl of T7 RNA polymerase, which were incubated at 42°C for 3 h. The amplified RNA was purified with RNeasy Mini Kits (Qiagen, Valencia, CA, USA). T7 RNA polymerase-amplified RNA (aRNA) from control mix and SALS was labeled with Cy3 and Cy5 fluorescence dyes, respectively, using the Atlas Glass Fluorescent Labeling Kit (Clontech, Palo Alto, CA, USA).

Cy3- and Cy5-labeled probes were hybridized to the custom-spotted arrays described above at 62°C for 16 h in a solution of 2×Denhardt's solution, 4×SSC and 0.2% SDS. After hybridization the arrays were washed in 2×SSC-0.1% SDS and 0.2×SSC for 20 min, respectively, and then rinsed with 0.2×SSC and 0.05×SSC. The slides were air-blown dried and prepared for scanning. The microarrays were scanned for fluorescence with GenePix (Axon, Union City, CA, USA).

2.4. Real-time RT-PCR

First-strand cDNA was synthesized from total RNA (1 μg) using 20 U Superscript II. Real-time RT-PCR was carried out using iCycler system (Bio-Rad Laboratories, Hercules, CA, USA) as described elsewhere [9]. All experiments were carried out in quadruplicate, and several negative controls were included. Fluorescence emission spectra were continuously monitored and analyzed with sequence detection software. For internal standard control, the expression of glyceraldehyde-3-phosphate dehydrogenase (GAPDH) was quantified simultaneously.

Primers and probe sequences (forward primer, reverse primer, and TaqMan probe): [GAPDH] 5′-CCT GGA GAA ACC TGC CAA GTA T-3′, 5′-TGA AGT CGC AGG AGA CAA CCT-3′, 5′-CAT CAA GAA GGT GGT GAA GCA GGC ATC-3′; [clone 1] 5′-CCG TCA CTC AAA AGG TTG AA-3′, 5′-TGG CGT GTG AAG TGA CTT TT-3′, 5′-AGC ATG AAG AGA CCT TTG AGG AGA AAC TAG TG-3′; [clone 2] 5′-AAG AGC AAG GAC CGC AAG TA-3′, 5′-GGG TGG CTC AGG TGA AGT AG-3′, 5′-CTC AGC GAG TAT GGC ATC AAT GTG AAG AAG-3′; [clone 3] 5′-TAG GAG CCA TCC GAG ACA AC-3′, 5′-TAC CAT GGC ACT TCC TGA CA-3′, 5′-CAC TAG CTG GAG CCA GTA TAA CGG GGA-3′; [clone 4] 5′-GAA GCT GAA GCA GGA TCA AA-3′, 5′-AGG GAG CAG CTT TCA CCT AT-3′, 5′-AAG TCC TTA AGA AAG CTG GGC TTG CCC AC-3′; [clone 5] 5′-GCC TGT TCT GTC ACC ATC AA-3′, 5′-GCA GAG GCC ACA GGT TTA GA-3′, 5′-CCA TTC AGC AGT CCA TTG AAA GGC TCT TAG-3′; [clone 6] 5′-CCT GTT GGA GGA GCA GAA CT-3′, 5′-GAA GCC ACA GAC AGC ACA GA-3′, 5′-AGG GCC CTA ACT ACC TGA CGG CCT GT-3′; [clone 7] 5′-GTT GAC CGA GCT GGA GAA AG-3′, 5′-CCT GTA GAC GGC ATG GAA AT-3′, 5′-CAT CGA CGT CTA CCA CAA GTA CTC CCT GAT-3′; [clone 8] 5′-AAG TGC GAG GGA TGC AAA T-3′, 5′-ACA CAG TCC TTG GCA CAC TT-3′, 5′-ACC TCC TGC AAG AAG AGC TGC TGC TC-3′; [clone 9] 5′-TCC CTT GAT CCC ACA AGT TC-3′, 5′-ACA GGC ATA CAC CAC CAC AT-3′, 5′-AGG CAG CAT AGT GAG ACC CCC ATC TCT ATA-3′; [clone 10] 5′-AGC TGC AGA ACA AGG AGC AT-3′, 5′-GTG AAG CCC CAC TTC TTT GA-3′, 5′-AGT TCA AGT TTC CTG GCC GCC AGA AGA T-3′; [clone 11] 5′-ACT GGT ACC CGT TGG AAC AA-3′, 5′-GTT CAT CCC ATC GTG GAT TT-3′, 5′-TGG TAC ACG ATT TTT AAG GAC CAC GTG TCT-3′.

Table 1
Details of patients

Patient	Age at death (years)	Sex	Postmortem interval (hours)	Disease duration (months)
ALS1	79	F	6	36
ALS2	67	F	6	48
ALS3	47	F	6	17
ALS4	74	M	6	45
ALS5	65	M	7	56
ALS6	57	M	5	48
ALS7	59	F	3	16
ALS8	57	M	6	68
C1	57	M	2	
C2	72	M	4.5	
C3	78	M	4.5	
C4	52	F	6	
C5	75	M	3	
C6	65	F	6	
C7	48	M	6	
C8	42	M	9	
ALS Ave.	63.1 ± 10.3		5.6 ± 1.2	
Control Ave.	61.1 ± 13.4		5.1 ± 2.2	

ALS1–8 are SALS patients. C1–8 are controls without neurological diseases.

Table 2
Candidate fragments from molecular indexing

	Up-regulated in ALS	Down-regulated in ALS	Total
BLAST matched genes	35	23	58
EST	6	11	17
Genome data base	5	4	9
Total	46	38	84

Molecular indexing yielded 84 candidate genes differentially expressed in SALS spinal cord compared with control spinal cord.

2.5. Statistics

Because of the size and distribution of the samples, a non-parametric two-tailed test was chosen (Mann–Whitney *U*-test). Significant values were calculated using StatView software (Hulinks, Tokyo, Japan).

3. Results and discussion

3.1. Molecular indexing and subsequent cDNA microarray analysis

Molecular indexing is a modified version of differential display. Compared with commercially based cDNA microarrays, these PCR-based screening procedures have the advantage of being able to cover an unrestricted range of expressed genes and to detect mRNAs of low abundance [10]. On the other hand, only one or a very limited number of samples can be practicably screened. Compared with conventional differential displays, this technique displays genes with the least redundancy and is less sensitive to the quality of RNA, which is advantageous in handling clinical materials [7,8].

The 576 electropherograms obtained from the SALS spinal cords were compared to control spinal cords. Eighty-four fragments with obvious differences in intensity were obtained. Forty-six of the 84 fragments showed stronger expression in the SALS spinal cord. The other 38 were highly expressed in the control spinal cord. Among the 84 fragments, 58 matched known genes in BLAST searches, 17 were expressed sequence tags (ESTs) and nine matched neither known genes nor ESTs (Table 2).

For the second screening, we spotted the 84 fragments on glass arrays and hybridized fluorescent aRNA from the SALS and control spinal cords (ALS1–5 and C1–5) on the arrays. The aRNA samples of all the control cases were mixed and used for the comparison with each SALS case. The expression ratio was calculated by dividing the fluorescence intensity of gene elements in each SALS sample by the fluorescence intensity of gene elements in the control mix. Several genes markedly altered their expression levels in the spinal cords between SALS and control mix (Fig. 1). Genes whose expression was consistently different (ratio of more than 2.0 or less than 0.5, SALS/control) between each SALS case and control mix were selected as the second candidates. Four genes showed stronger signals (clones 1–4) and seven showed weaker signals (clones 5–11) in the SALS spinal cords (Table 3).

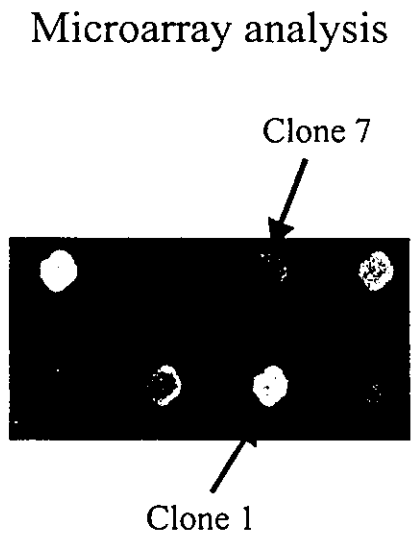

Fig. 1. Close-up image of microarray. Two different fluorescence dyes, Cy3 and Cy5, were on the array together. A stronger Cy3 signal (green) indicates down-regulation and a stronger Cy5 signal (red) indicates up-regulation in SALS. For example, clone 1 shows an orange color, implying down-regulation, whereas clone 7 with a green color is up-regulated in SALS compared to control.

3.2. Verification of candidate genes by real-time RT-PCR

The expression of 11 candidate clones in the SALS and the control spinal cords was examined by real-time RT-PCR using TaqMan probes. Six clones were determined to have significantly different expression in the SALS spinal cords. Three clones (2, 3 and 4) were significantly up-regulated in SALS cases compared with controls ($P < 0.05$), and the other three clones (7, 8 and 11) showed significantly lower expression in SALS cases than in controls ($P < 0.05$). However, clones 1, 5, 6, 9 and 10 showed no significant difference (Fig. 2).

A similarity search revealed that clones 2, 7, 8 and 11 were identical to four known cDNAs, 30-kDa TATA-binding protein-associated factor (TAFII30), macrophage-inhibiting factor-related protein-8 (MRP8), metallothionein-3 (MT-3) and ubiquitin-like protein 5 (UBL5), respectively. Clones 3 and 4 proved to be identical to ESTs. We cloned these two unknown

Table 3
Gene expression on microarray analysis

Clone number	Expression ratio (ALS/control)
1	2.94 ± 1.33
2	2.67 ± 1.41
3	2.39 ± 1.21
4	2.12 ± 0.77
5	0.44 ± 0.19
6	0.28 ± 0.14
7	0.27 ± 0.21
8	0.36 ± 0.18
9	0.35 ± 0.16
10	0.33 ± 0.15
11	0.45 ± 0.25

Data are means ± S.D. of five different SALS case/control mixes. Genes whose expression was consistently different (ratio of more than 2.0 or less than 0.5, SALS/control) between each SALS case and control mix were selected as the second candidates.

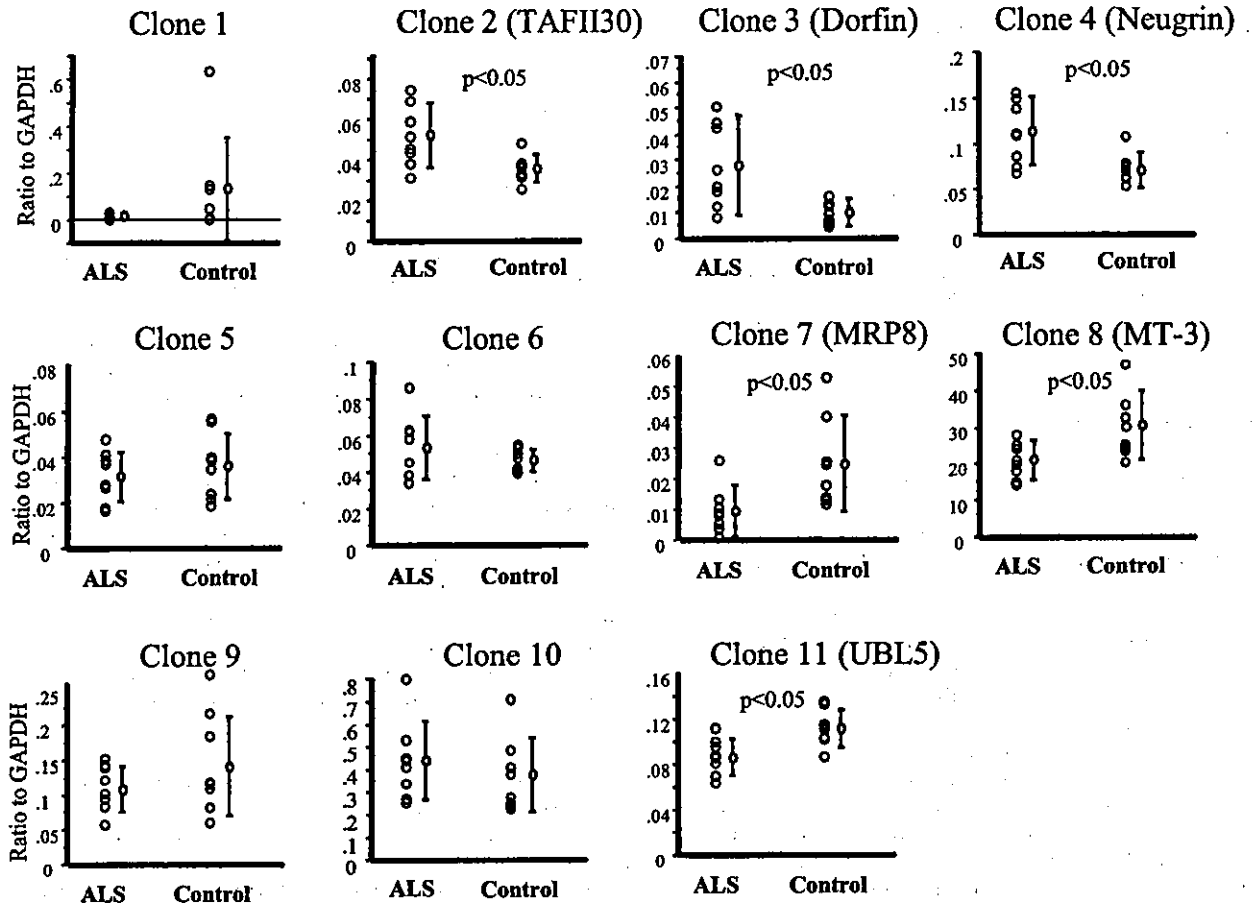

Fig. 2. Verification of SALS-specific gene expression by real-time RT-PCR. The expression level is shown as the weight ratio of the target gene to GAPDH. Quantification of standard templates and each sample was determined by four different experiments. Eight samples each of SALS and controls were examined. Values are the means ± S.D., $n = 8$; statistics were carried out by Mann–Whitney U-test. There were significant differences between SALS and control in clones 2, 3, 4, 7, 8 and 11 ($P < 0.05$). No significant difference was found for other clones.

genes using RACE methods and named them dorfin and neugrin in previous reports [11,12].

TAFII30 is one of the TATA-binding protein-associated factors required for transcription of a subset of genes [13]. An immunohistochemical study using SCA7 transgenic mice showed that TAFII30 is accumulated in nuclear inclusions in neurons. The trapping of this transcription initiation factor in nuclear inclusions may alter the activity of cellular transcription, and contribute to neuronal toxicity in SCA7 model mice [14]. Our result showed up-regulation of the TAFII30 gene in the SALS spinal cords, which suggests that this molecule may also be involved in SALS pathophysiology. More investigation is necessary to clarify whether up-regulation of this molecule has a pivotal role in SALS or only reflects some disruption of transcription function occurring in SALS.

Dorfin is a new RING finger-type ubiquitin ligase, containing two RING finger motifs and an IBR motif at its N-terminus. This gene is ubiquitously expressed in central nervous system tissues [11]. Our recent study showed that dorfin is localized in the ubiquitinated inclusions of FALS and SALS, bound and ubiquitinated various mutant forms of SOD1 in vitro, and protected from mutant SOD1-mediated neurotoxicity in mutant SOD1 culture cells [15]. These results indicate that dorfin has a crucial role in the pathomechanism of mutant SOD1-mediated FALS. In the present study we showed that the expression of the dorfin gene was significantly higher in the SALS than in the control spinal cords. Considering that it has a protective function in FALS and is localized in inclusions of SALS, dorfin may play some protective role in the pathogenesis of SALS as well. Since some authors consider that misfolded protein generally play a central role in various neurodegenerative disorders, such as Huntington disease, Alzheimer disease, Parkinson disease, familial spinocerebellar degeneration and ALS [16], dorfin may possibly work to eliminate proteins which are toxic to motor neurons in the SALS spinal cord.

The expression of neugrin increases with the process of neuronal differentiation. This gene is strongly expressed in the nervous system and mainly in neurons in the spinal cord [12]. These results indicate that up-regulation of this gene in the SALS spinal cord reflects gene expression changes in dying neurons, not in reactive proliferation of glial cells. However, the potential role of neugrin remains to be elucidated.

MRP8 is mainly expressed in microglial cells in neuronal tissues, and it is up-regulated with microglial activation, such as traumatic injury or viral infection [17,18]. MRP8 decreased in the SALS spinal cords in the present study. This is paradoxical because gliosis is one of the hallmarks in ALS path-